J. Mech. Phys. Solids 180 (2023) 105403

Contents lists available at ScienceDirect

Journal of the Mechanics and Physics of Solids

journal homepage: www.elsevier.com/locate/jmps

A general model for anisotropic pseudo-elasticity and viscoelasticity at finite strains

Maximilian P. Wollner [a], Michele Terzano [a], Malte Rolf-Pissarczyk [a], Gerhard A. Holzapfel [a,b,*]

[a] Institute of Biomechanics, Graz University of Technology, Graz, Austria
[b] Department of Structural Engineering, Norwegian University of Science and Technology, Trondheim, Norway

ARTICLE INFO

Keywords:
Continuum mechanics
Material modeling
Anisotropy
Structure tensor
Pseudo-elasticity
Finite viscoelasticity

ABSTRACT

Given the growing demand for simulating anisotropic material behavior at finite strains, constitutive modeling is in a challenging position to combine descriptive capabilities for several inelastic phenomena with the numerical feasibility for real-world applications. In this article, we develop a material model capable of reproducing anisotropy, viscoelasticity, stress softening, and permanent set by merging several pre-existing frameworks. Each constitutive effect is discussed separately in terms of its thermodynamics and mechanical interpretation and successively built on top of each other. Here, the pseudo-elastic approach to permanent set occupies a special place, with a novel discussion of its applicability to generic deformations. We show that the formulation does not lead to physical behavior in general, but can be constrained in such a way to produce appropriate stress predictions in an average sense. Examples of the stress response in several different deformation modes are visualized throughout. The capabilities and possible shortcomings of the formulation are highlighted and at the end a simple numerical algorithm for stress computation is presented.

1. Introduction

Anisotropic material models at finite strains are experiencing ever increasing demand in commercial applications such as fiber-reinforced soft composites (Reese, 2003), tissue-engineered materials (Li et al., 2019; Szafron et al., 2019), and textiles (Pierrat et al., 2021). While considerable effort has been put into modeling soft fibrous tissues, see Humphrey (2003), Holzapfel and Ogden (2009), Li (2016), Lanir (2017) and Holzapfel et al. (2019), these approaches are not necessarily applicable to synthetic materials. To make matters worse, inelastic effects, e.g., viscoelasticity, stress softening, and permanent set are in many cases so pronounced that a simple hyperelastic formulation is insufficient for a valid approximation, see, e.g., Miehe and Keck (2000), Diani et al. (2009), Baker et al. (2009) and Vernerey (2018).

In this study we attempt to combine several already existing modeling approaches to describe anisotropic material behavior including all inelastic effects listed above. For this purpose, each aspect of the model is discussed separately, successively building on each other. Although the resulting formulation is easy to implement, see Appendix D, there are considerable nuances in terms of thermodynamics and mechanical interpretability in each building block. We begin by introducing certain general continuum-mechanical quantities in Section 2, which will be used throughout. For the most part, symbolic tensor notation is employed, although a switch to index notation can be beneficial.

* Corresponding author at: Institute of Biomechanics, Graz University of Technology, Graz, Austria.
E-mail address: holzapfel@tugraz.at (G.A. Holzapfel).

https://doi.org/10.1016/j.jmps.2023.105403
Received 18 April 2023; Received in revised form 8 July 2023; Accepted 2 August 2023
Available online 10 August 2023

All inelastic effects reference the quasi-static, purely elastic formulation in some form, such that a closer discussion thereof is required. Therefore, in Section 3, we adapt an anisotropic hyperelastic model introduced by Itskov and Aksel (2004) and Ehret and Itskov (2007) that employs structure tensors to describe classes of material symmetries. These tensors can also be interpreted as probabilistic quantities, see, e.g., Driessen et al. (2003) and Gasser et al. (2006), which provide a pathway to the concepts of the principle of minimum averaged free energy and non-affine deformation, see Miehe et al. (2004) and Tkachuk and Linder (2012). A worthwhile review of this topic can be found in Britt and Ehret (2022). Therewith closely related is the topic of convexity, more precisely polyconvexity. At this point, we refer to Balzani et al. (2006), Schröder (2010) or Krawietz (1986, chap. 12), the latter of which gives a more physically motivated introduction to the topic, albeit in German.

The constitutive behavior is assumed to be incompressible. In addition to the advantages in the numerical implementation for shell elements, this feature captures the *in vivo* behavior of blood-filled polymer scaffolds for which this model was originally developed. An extension to compressible, inelastic material behavior is possible for all formulations in this study, but we mention that the application of the isochoric-volumetric split in the case of anisotropy is a delicate issue, as pointed out in Sansour (2008), and should be employed with caution, if at all.

In Section 4 we discuss the modeling of stress softening, also known as the Mullins effect, see Mullins (1948). At its center rests the experimental fact that some materials exhibit a certain constitutive behavior on the primary loading path and then become more compliant, i.e. damaged, during unloading and reloading until the primary loading path is reached again, upon which the material recovers as if it had not been damaged at all. A widely used, so-called pseudo-elastic, constitutive framework is provided by Ogden and Roxburgh (1999), which lacks a corresponding thermodynamic discussion subsequently remedied by Naumann and Ihlemann (2015) without changing the core of the original model. We follow the approach with some minor adjustments.

The above-mentioned pseudo-elastic formulation is extended in Dorfmann and Ogden (2004) and Fereidoonnezhad et al. (2016) to include permanent set, i.e. residual deformation, even if its validity for general deformations is not discussed. Nonetheless, the approach appears attractive due to its simple implementation compared to more elaborate models such as Göktepe and Miehe (2005) and Itskov et al. (2010). We therefore explore the capabilities of the pseudo-elastic formulation including permanent set for general anisotropic material behavior in Section 5.

For the modeling of viscoelasticity in Section 6, we closely follow Liu et al. (2021), which in turn is based on Simo (1987) and Holzapfel and Simo (1996). These formulations are referred to as finite linear viscoelasticity, alluding to the linearity of the underlying evolution equations, with the advantage that an interpretation in terms of Maxwell elements is still applicable, although only small deviations from thermodynamic equilibrium are valid. A computational advantage over models that use a multiplicative split of the deformation gradient, such as Reese and Govindjee (1998) and Ciambella and Nardinocchi (2021), is the relative ease of implementation in case of anisotropy, since the multiplicative approach requires a more thorough treatment of structural-frame indifference, see, e.g., Casey (2017) and Holthusen et al. (2023). For a detailed discussion of the advantages and disadvantages of both approaches, the reader is referred to the introduction in Liu et al. (2021).

In Section 7 we summarize the proposed model with reference to the relevant expressions and give an overview of the material parameters. We also briefly discuss a possible calibration of the model and the consequences for the design of mechanical experiments. Section 8 contains more application examples of the model to illustrate its capabilities as well as possible shortcomings. We end the paper with a short conclusion in Section 9.

In general, details and considerations deemed non-obvious by the authors are highlighted as remarks throughout. All relevant relations are implemented in the programming language Julia, see Bezanson et al. (2017).

2. Continuum-mechanical preliminaries

2.1. Kinematics

A material body $\mathcal{B}$ is a set of particles traversing different configurations according to a bijective mapping $\boldsymbol{x} = \boldsymbol{\chi}(\boldsymbol{X}, t)$, which relates the positional vectors $\boldsymbol{X} \in \Omega_0$ and $\boldsymbol{x} \in \Omega$ in the reference configuration $\Omega_0 \subset \mathbb{R}^3$ and the current configuration $\Omega \subset \mathbb{R}^3$, respectively, for some time $t \geq 0$. With this, we can define the deformation gradient

$$\mathbf{F} = \boldsymbol{\nabla}_{\boldsymbol{X}} \boldsymbol{\chi} \qquad \text{alongside its determinant} \qquad J = \det \mathbf{F} > 0 \tag{1}$$

and the right Cauchy–Green tensor

$$\mathbf{C} = \mathbf{F}^{\mathrm{T}} \mathbf{F}, \tag{2}$$

see, e.g., Truesdell and Noll (1965, sec. C.I–II).

Since the material is assumed to be incompressible, i.e. $J = 1$, we also introduce the isochoric-volumetric split, i.e.

$$\overline{\mathbf{F}} = J^{-1/3} \mathbf{F} \qquad \text{with} \qquad \det \overline{\mathbf{F}} = 1 \qquad \text{and} \qquad \overline{\mathbf{C}} = \overline{\mathbf{F}}^{\mathrm{T}} \overline{\mathbf{F}}, \tag{3}$$

cf. Flory (1961, eq. 9).

2.2. Thermodynamics

For the purposes of this study, the material is assumed to be isothermal, so a discussion of temperature-related effects is omitted. Inertial effects and moment densities are also neglected. We assume the existence of a free-energy function $\Psi = \Psi(\mathbf{C}, \dots)$, where the dots represent any number of internal variables and parameters that must satisfy the Clausius–Duhem inequality

$$\mathcal{D} = \frac{1}{2}\mathbf{S} : \dot{\mathbf{C}} - \dot{\Psi} \geq 0, \tag{4}$$

where $\mathcal{D}$ denotes the dissipation (density) and $\mathbf{S}$ the second Piola–Kirchhoff stress tensor, see, e.g., Eringen (1980, chap. 4). In addition, the function Ψ adheres to material frame invariance, see, e.g., Truesdell and Noll (1965, eq. 19.2). Notationally, $(\dot{\cdot})$ indicates differentiation with respect to time t and $(\cdot) : (\cdot)$ double contraction. The Clausius–Duhem inequality (4) itself does not constitute a field equation, but rather serves as a guiding principle for the validity of dissipative constitutive formulations.

With incompressibility and the decomposition (3) in mind, we assume an additive split of Ψ into an isochoric and a volumetric part in the form

$$\Psi(\mathbf{C}, \dots) = \Psi_{\text{iso}}(\overline{\mathbf{C}}, \dots) + \Psi_{\text{vol}}(J), \tag{5}$$

where any inelastic effects and thus internal variables, represented by dots in (5), are only introduced with respect to the isochoric response. We emphasize that for the purposes of this study, the volumetric part only serves as a numerical means to establish near-incompressibility through a penalty method in a computational context. For perfect incompressibility, $\Psi_{\text{vol}}(J) = -p(J-1)$, where p denotes a Lagrange parameter. Even then, it can be advantageous to continue working with the unimodular right Cauchy–Green tensor $\overline{\mathbf{C}}$. Although this does not play a role for the incompressible limit, it can still influence the convergence behavior in the computational context, see, e.g., Gültekin et al. (2019). By construction, the energy function is set to zero in the initial, undeformed configuration, i.e. $\Psi(\mathbf{I}, \dots) = 0$, where $\mathbf{I}$ denotes the second-order unit tensor. Similarly, we require the body to be stress free, i.e. $\partial\Psi/\partial\mathbf{C} = \mathbf{0}$ evaluated at $\mathbf{C} = \mathbf{I}$. We emphasize that these conditions only have to be fulfilled in the undeformed configuration at $t = 0$. For any subsequent returns to $\mathbf{C} = \mathbf{I}$ at $t > 0$ these conditions need not hold in general due to inelastic effects.

3. Anisotropic hyperelasticity

Here we introduce an anisotropic hyperelastic material model on which the inelastic effects are built. The section consists of three subsections. First, we discuss the concept of structure tensors to model anisotropy from both a geometrical and probabilistic point of view, independent of any mechanics. Then we use these quantities to define anisotropic invariants, which in turn are arguments for a free-energy function, from which we acquire an expression for the purely elastic stress response. Because these invariants inherit the probabilistic nature of structure tensors, they all have a physical meaning. Finally, we use this interpretability to illustrate a principle of minimum averaged free energy that does not alter the hyperelastic formulation itself, but provides additional motivation for using a formalism based on structure tensors.

3.1. Structure tensors

As can be seen in Ehret and Itskov (2007, eq. 18), we introduce anisotropy by defining a symmetric, positive semi-definite generalized structure tensor in its spectral form, i.e.

$$\mathbf{H} = \sum_{k=1}^{n} H_k \mathbf{L}_k \qquad \text{with} \qquad \sum_{k=1}^{n} \mathbf{L}_k = \mathbf{I} \qquad \text{and} \qquad \operatorname{tr}\mathbf{H} = \sum_{k=1}^{n} H_k = 1, \tag{6}$$

where $n \in \{1, 2, 3\}$, depending on the algebraic multiplicity of the eigenvalues $0 \leq H_k \leq 1$, which together with their corresponding projection tensors $\mathbf{L}_k$ encapsulate the specific type of anisotropy, i.e. isotropy for $n = 1$, transverse isotropy for $n = 2$, and orthotropy for $n = 3$. More complex material symmetries require structure tensors of higher order, see, e.g., Zheng (1994, chap. 3), which will not be discussed here. Each structure tensor $\mathbf{H}$ is then defined by at most five independent parameters because of its normalized trace.

Another more illustrative way to define a structure tensor is in a probabilistic manner, as carried out by Gasser et al. (2006, eq. 3.14). There,

$$\mathbf{H}_{\parallel} = \mathbb{E}[\boldsymbol{N} \otimes \boldsymbol{N}] = \frac{1}{4\pi} \int_{\mathcal{S}} \boldsymbol{N} \otimes \boldsymbol{N} \rho(\boldsymbol{N}) \, \mathrm{d}\mathcal{S}, \tag{7}$$

i.e. the expected value $\mathbb{E}[(\cdot)]$ of the dyadic product of the unit vector $\boldsymbol{N}$ for a given probability density $\rho(\boldsymbol{N})$ of possible fiber orientations defined over the surface of the unit sphere $\mathcal{S}$. The normalization of $\rho(\boldsymbol{N})$ ensures the identity trace of $\mathbf{H}_{\parallel}$. The '$\parallel$'-subscript emphasizes that the unit vectors $\boldsymbol{N}$ lie coaxially to the physical fiber direction. Since fiber-like constituents are nonetheless three-dimensional structures, it makes sense to attempt to also capture their transverse orientations, i.e. all directions orthogonal to $\boldsymbol{N}$. For this purpose, the projection tensor $\mathbf{I} - \boldsymbol{N} \otimes \boldsymbol{N}$ encapsulates all vectors lying in the plane with the normal $\boldsymbol{N}$, cf. Schröder and Neff (2003, eq. 3.25). A straightforward approach is then to introduce an additional structure tensor in the form

$$\mathbf{H}_{\perp} = \mathbb{E}\Big[\frac{1}{2}(\mathbf{I} - \boldsymbol{N} \otimes \boldsymbol{N})\Big] = \frac{1}{4\pi} \int_{\mathcal{S}} \frac{1}{2}(\mathbf{I} - \boldsymbol{N} \otimes \boldsymbol{N}) \rho(\boldsymbol{N}) \, \mathrm{d}\mathcal{S} = \frac{1}{2}\big(\mathbf{I} - \mathbf{H}_{\parallel}\big), \tag{8}$$

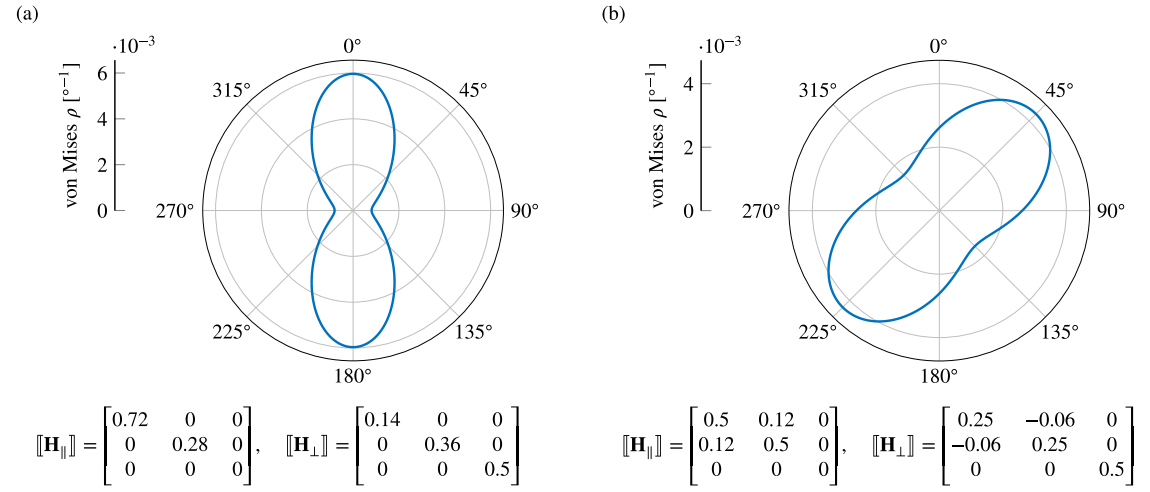

Fig. 1. Polar plots of two π-periodic von Mises distributions $\rho(\varphi) \propto \exp\{\kappa \cos[2(\varphi - \varphi_0)]\}$, cf. Evans et al. (2000, chap. 41), with (a) $\kappa = 1$, $\varphi_0 = 0°$ and (b) $\kappa = 0.5$, $\varphi_0 = 45°$ and the corresponding structure tensors in matrix representation. The tilted axis of symmetry in (b) is reflected in the non-diagonal entries of $\mathbf{H}_\parallel$. The three-dimensional nature of $\mathbf{H}_\perp$ indicates that, although all fibers are in-plane, they still have an extension normal to the plane, i.e. $\mathbf{H}_\perp$ captures all direction lying in the planes normal to the fibers in an average sense.

where the last step follows from the linearity of expectation. The factor $1/2$ takes care of the normalization and reflects the planar space of the possible transverse directions. Therefore, $\mathbf{H}_\perp$ can be interpreted as the expected value of all transverse directions lying in the plane normal to $\boldsymbol{N}$ given some fiber distribution $\rho(\boldsymbol{N})$. By comparison with (6), it is evident that $\mathbf{H}_\perp$ itself constitutes a generalized structure tensor. Consequently, $\mathbf{H}_\parallel$ and $\mathbf{H}_\perp$ are interdependent and one determines the other. The advantage is that both the coaxial and the transverse fiber constitutive behavior can now be modeled more tangibly.

Fig. 1 illustrates the interaction of a fiber distribution $\rho(\boldsymbol{N})$ and the resulting structure tensor $\mathbf{H}_\parallel$ using two distinct, planar π-periodic von Mises distributions. Although in these cases no fibers are oriented out-of-plane, they still have an extension in that direction, as indicated by the three-dimensional nature of $\mathbf{H}_\perp$, see (8).

Remark 1. Note that for calibration purposes, knowledge of $\rho(\boldsymbol{N})$ is not essential, but beneficial. Either one of the structure tensors can simply be treated as five additional material constants, the number of which can be further reduced given the planes of material symmetry.

Remark 2. Because each coaxial direction has an associated transverse behavior, there is no need for an isotropic ground matrix embedding fibers as is the case in, e.g., Gasser et al. (2006).

3.2. Polyconvex formulation

For the definition of the isochoric free-energy function $\Psi_{\text{iso}}^{0,\infty}$ for the undamaged body in equilibrium, hence the superscripts, we use the polyconvex formulation of Itskov and Aksel (2004, eq. 84), with a slightly different parameterization in the form

$$\Psi_{\text{iso}}^{0,\infty}(\overline{\mathbf{C}}) = \frac{1}{2} \sum_{p \in \{\parallel, \perp\}} \mu_p \left[\frac{1}{\gamma_p + 1} \left(\overline{K}_{1p}^{\gamma_p + 1} - 1 \right) + \frac{1}{\delta_p + 1} \left(\overline{K}_{-1p}^{\delta_p + 1} - 1 \right) \right], \tag{9}$$

where $\overline{K}_{\pm 1p}$ are four isochoric invariants defined as

$$\overline{K}_{1p} = \mathbf{H}_p : \overline{\mathbf{C}} \qquad \text{and} \qquad \overline{K}_{-1p} = \mathbf{H}_p : \overline{\mathbf{C}}^{-1} \qquad \text{for} \qquad p \in \{\parallel, \perp\}, \tag{10}$$

which all have a meaningful physical interpretation.

The macroscopic, isochoric deformation of a single line element along the unit vector $\boldsymbol{N}$ follows from the well-known dot product $\lambda_\parallel^2 = (\overline{\mathbf{F}}\boldsymbol{N}) \cdot (\overline{\mathbf{F}}\boldsymbol{N}) = (\boldsymbol{N} \otimes \boldsymbol{N}) : \overline{\mathbf{C}}$, cf. Miehe et al. (2004, eq. 33). Given the distribution $\rho(\boldsymbol{N})$, we can then calculate the expected value for $\lambda_\parallel^2$ by noticing that

$$\mathbb{E}\left[\lambda_\parallel^2\right] = \mathbb{E}\left[(\boldsymbol{N} \otimes \boldsymbol{N}) : \overline{\mathbf{C}}\right] = \mathbb{E}[\boldsymbol{N} \otimes \boldsymbol{N}] : \overline{\mathbf{C}} = \mathbf{H}_\parallel : \overline{\mathbf{C}} = \overline{K}_{1\parallel} \tag{11}$$

with the help of (7). Likewise, an area element with the normal $\boldsymbol{N}$ changes macroscopically for an isochoric deformation according to $\nu_\parallel^2 = (\overline{\mathbf{F}}^{-\mathrm{T}}\boldsymbol{N}) \cdot (\overline{\mathbf{F}}^{-\mathrm{T}}\boldsymbol{N}) = (\boldsymbol{N} \otimes \boldsymbol{N}) : \overline{\mathbf{C}}^{-1}$, cf. Miehe et al. (2004, eq. 58); in particular, $\overline{\mathbf{C}}^{-1} = \operatorname{cof} \overline{\mathbf{C}}$. Then,

$$\mathbb{E}\left[\nu_\parallel^2\right] = \mathbb{E}\left[(\boldsymbol{N} \otimes \boldsymbol{N}) : \overline{\mathbf{C}}^{-1}\right] = \mathbb{E}[\boldsymbol{N} \otimes \boldsymbol{N}] : \overline{\mathbf{C}}^{-1} = \mathbf{H}_\parallel : \overline{\mathbf{C}}^{-1} = \overline{K}_{-1\parallel}. \tag{12}$$

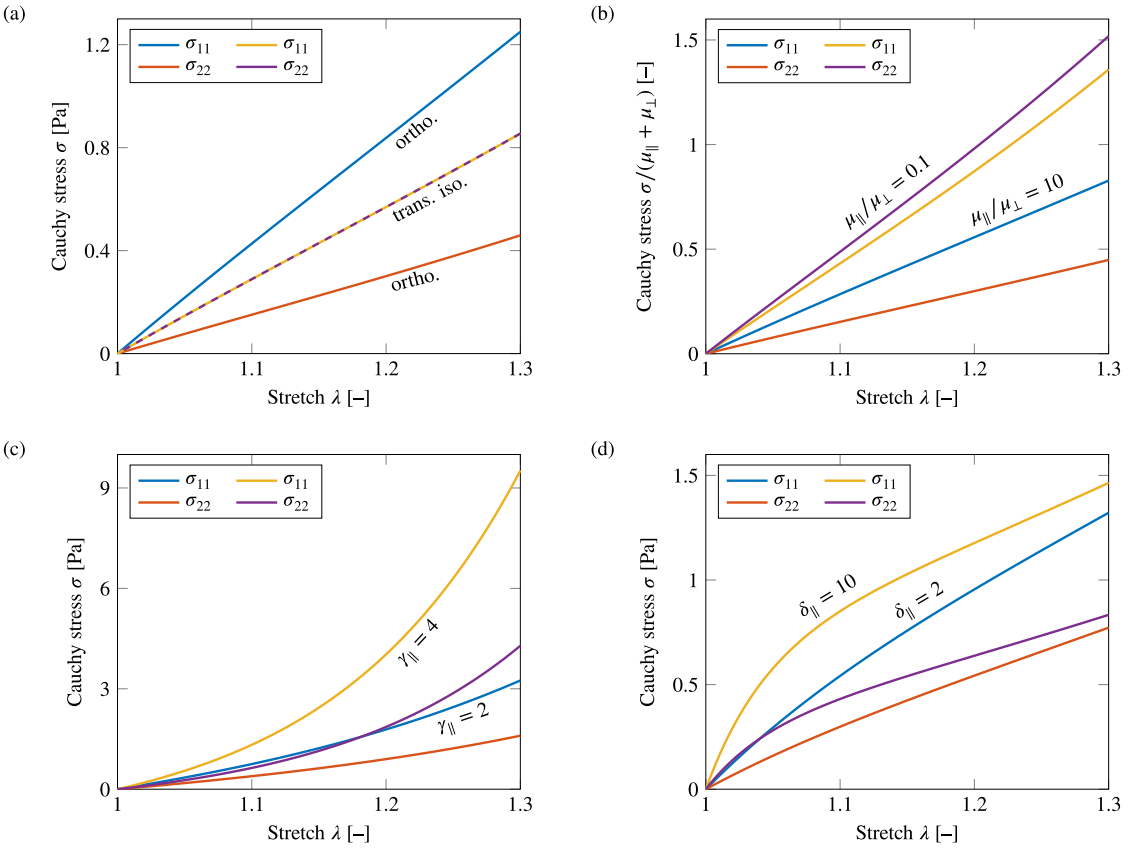

Fig. 2. Quasi-static, non-dissipative, equibiaxial stress response for different parameter combinations. Unless otherwise stated in the plot, $\theta_{0,\infty} = (0.7, 0.3, 1\,\text{Pa}, 0.2\,\text{Pa}, 0, 0, 0, 0)$. (a) Only the type of anisotropy is altered, recovering the transversely isotropic behavior for $H_1 = H_2 = 0.5$ and the orthotropic behavior for $H_1 = 0.9$ and $H_2 = 0.1$. Notice the overlapping trajectories in the former case. (b) The effect of the ratio between the coaxial and transverse stiffness, $\mu_\parallel$ and $\mu_\perp$, is illustrated. The direction with the most fibers does not necessarily correspond to the stiffest stress response. (c) Increasing only $\gamma_\parallel$ leads to a more progressive stiffness evolution for that particular deformation mode. (d) Increasing only $\delta_\parallel$ leads to a degression of stiffness, analogous to (c).

The expressions (11) and (12) carry over analogously to the transverse structure tensor $\mathbf{H}_\perp$. Here the invariants $\overline{K}_{1\perp}$ and $\overline{K}_{-1\perp}$ capture the expected macroscopic isochoric deformation of line and area elements, $\lambda_\perp^2 = (\mathbf{I} - \boldsymbol{N}\otimes\boldsymbol{N})/2 : \overline{\mathbf{C}}$ and $\nu_\perp^2 = (\mathbf{I} - \boldsymbol{N}\otimes\boldsymbol{N})/2 : \overline{\mathbf{C}}^{-1}$, in the plane perpendicular to the fiber direction $\boldsymbol{N}$, respectively, i.e.

$$\begin{aligned}\mathbb{E}\left[\lambda_\perp^2\right] &= \mathbb{E}\left[\frac{1}{2}(\mathbf{I} - \boldsymbol{N}\otimes\boldsymbol{N}) : \overline{\mathbf{C}}\right] = \mathbf{H}_\perp : \overline{\mathbf{C}} = \overline{K}_{1\perp},\\ \mathbb{E}\left[\nu_\perp^2\right] &= \mathbb{E}\left[\frac{1}{2}(\mathbf{I} - \boldsymbol{N}\otimes\boldsymbol{N}) : \overline{\mathbf{C}}^{-1}\right] = \mathbf{H}_\perp : \overline{\mathbf{C}}^{-1} = \overline{K}_{-1\perp}.\end{aligned} \tag{13}$$

We emphasize that for the definition of the transverse quantities we never define a particular vector orthogonal to $\boldsymbol{N}$, but always refer to the plane with the normal $\boldsymbol{N}$ containing all possible orthogonal vectors encapsulated by the projection tensor $\mathbf{I} - \boldsymbol{N}\otimes\boldsymbol{N}$.

Assuming that only isochoric deformations are applicable, sufficient conditions to ensure polyconvexity are $\mu_\parallel \geq 0$ and $\mu_\perp \geq 0$ for the stiffness-like parameters, which weight the coaxial and transverse contributions, and $\gamma_\parallel \geq 0$, $\delta_\parallel \geq 0$, $\gamma_\perp \geq 0$, and $\delta_\perp \geq 0$ for the shape parameters that control the influence of their associated invariants, cf. Itskov and Aksel (2004, eq. 59).

Inserting (5) and (9) into (4) and collecting the terms with $\dot{\mathbf{C}}$, we get the standard expression for the second Piola–Kirchhoff stress tensor $\mathbf{S}$, i.e.

$$\mathbf{S} = J^{-2/3}\mathbb{P} : \overline{\mathbf{S}}^{0,\infty} + \mathbf{S}_{\text{vol}}^{0,\infty} \tag{14}$$

with the fourth-order projection tensor $\mathbb{P} = \mathbb{I} - \mathbf{C}^{-1}\otimes\mathbf{C}/3$, where $\mathbb{I}$ denotes the fourth-order unit tensor defined as $(\mathbb{I})_{IJKL} = (\delta_{IK}\delta_{JL} + \delta_{IL}\delta_{JK})/2$. Then,

$$\overline{\mathbf{S}}^{0,\infty} = 2\frac{\partial \Psi_{\text{iso}}^{0,\infty}}{\partial \overline{\mathbf{C}}} = \sum_{p\in\{\parallel,\perp\}} \mu_p\left(\overline{K}_{1p}^{\gamma_p}\mathbf{H}_p - \overline{K}_{-1p}^{\delta_p}\overline{\mathbf{C}}^{-1}\mathbf{H}_p\overline{\mathbf{C}}^{-1}\right), \tag{15}$$

$$\mathbf{S}_{\text{vol}}^{0,\infty} = J\frac{\partial \Psi_{\text{vol}}^{0,\infty}}{\partial J}\mathbf{C}^{-1}, \tag{16}$$

where we leave $\Psi^{0,\infty}_{\text{vol}}$ unspecified, albeit under the assumption that incompressibility can be enforced either by a penalty function or by a Lagrange parameter. Other stress measures such as the first Piola–Kirchhoff (nominal) stress and the Cauchy (true) stress follow as usual according to $\mathbf{P} = \mathbf{FS}$ and $\boldsymbol{\sigma} = J^{-1}\mathbf{FSF}^{\mathrm{T}}$, respectively.

From now on, the eigenvectors of the structure tensors defining the planes of material symmetry coincide with the global coordinate system $(\boldsymbol{E}_k)_{k=1}^3$ in which the loading is specified, i.e. $\mathbf{L}_k = \boldsymbol{E}_k \otimes \boldsymbol{E}_k$. For implementation, this means the structure tensors have a diagonal matrix representation. Without loss of generality, we can use H_1 and H_2 from $\mathbf{H}_\parallel$ to prescribe the type of anisotropy. For orthotropy, all eigenvalues H_1, H_2, and $H_3 = 1 - H_1 - H_2$ must be distinct, while for transverse isotropy exactly two must be identical, e.g., $H_1 = H_2$ and $H_3 \neq H_1$. In the case of isotropy, $H_1 = H_2 = H_3 = 1/3$.

Fig. 2 shows four examples of the quasi-static, non-dissipative true stress response $\boldsymbol{\sigma}$ for equibiaxial extension. Incompressibility is ensured through the use of a Lagrange parameter. The material parameters form an octuple $\theta_{0,\infty} = (H_1, H_2, \mu_\parallel, \mu_\perp, \gamma_\parallel, \gamma_\perp, \delta_\parallel, \delta_\perp)$. It can be seen that the formulation can approximate different degrees of anisotropy mainly by adjustment of $H_1, H_2, \mu_\parallel$, and $\mu_\perp$, see Fig. 2(a),(b), as well as nonlinear stiffness progressions with the shape parameters $\gamma_\parallel, \gamma_\perp, \delta_\parallel$, and $\delta_\perp$, see Fig. 2(c),(d).

Remark 3. If $\gamma_p = \delta_p = 0$ and $\mu_\perp = 2\mu_\parallel$, the material behaves isotropically regardless of the choice of $\mathbf{H}_\parallel$.

Remark 4. In addition to Sansour (2008), the shortcomings of using the isochoric-volumetric split for compressible material behavior is further hinted at in Hartmann and Neff (2003, cor. 2.3) by the fact that the common isochoric invariant $\mathrm{tr}(\overline{\mathbf{C}}^{-1})$ is not polyconvex for general compressible deformations.

3.3. Principle of minimum averaged free energy

The requirement for polyconvexity can be closely related to a principle of minimum averaged free energy, as discussed in Miehe et al. (2004, sec. 4.3.2) or Tkachuk and Linder (2012, eq. 32), while simultaneously capturing the notion of non-affine deformation. To clarify, we might know that, given a macroscopic isochoric deformation $\overline{\mathbf{F}}$, the affine line deformation along a fiber $\boldsymbol{N}$ follows $\lambda_\parallel^2 = (\boldsymbol{N} \otimes \boldsymbol{N}) : \overline{\mathbf{C}}$ and that the representative affine area deformation along all vectors perpendicular to the fiber direction $\boldsymbol{N}$ reads $\nu_\perp^2 = (\mathbf{I} - \boldsymbol{N} \otimes \boldsymbol{N})/2 : \overline{\mathbf{C}}^{-1}$; however, for a given fiber network $\rho(\boldsymbol{N})$ the fibers do not necessarily have to deform affinely on the microscale to retrieve the expected macroscopic deformations $\overline{K}_{1\parallel}$ and $\overline{K}_{-1\perp}$.

Suppose now there are four such microscopic deformation fields $\widetilde{\lambda}_p^2(\boldsymbol{N}; \overline{\mathbf{F}})$ and $\widetilde{\nu}_p^2(\boldsymbol{N}; \overline{\mathbf{F}})$ that are yet to be determined functions. We can define a functional $\Psi^{0,\infty}_{\text{iso,avg}}$ that captures the average free energy for a given macroscopic isochoric deformation $\overline{\mathbf{F}}$ with

$$\begin{aligned}\Psi^{0,\infty}_{\text{iso,avg}}\left[\widetilde{\lambda}_\parallel^2, \widetilde{\nu}_\parallel^2, \widetilde{\lambda}_\perp^2, \widetilde{\nu}_\perp^2; \overline{\mathbf{F}}\right] &= \mathbb{E}\left[\Psi^{0,\infty}_{\text{iso}}(\widetilde{\lambda}_\parallel^2, \widetilde{\nu}_\parallel^2, \widetilde{\lambda}_\perp^2, \widetilde{\nu}_\perp^2)\right] \\ &= \frac{1}{4\pi}\int_S \Psi^{0,\infty}_{\text{iso}}(\widetilde{\lambda}_\parallel^2, \widetilde{\nu}_\parallel^2, \widetilde{\lambda}_\perp^2, \widetilde{\nu}_\perp^2)\rho(\boldsymbol{N})\,\mathrm{d}S,\end{aligned} \tag{17}$$

subject to the four constraints that the averaged microscopic deformation fields are equivalent to the expected macroscopic deformation fields from (11)–(13), i.e.

$$\begin{aligned}\mathbb{E}\left[\widetilde{\lambda}_p^2\right] = \mathbb{E}\left[\lambda_p^2\right] \quad &\Longrightarrow \quad \frac{1}{4\pi}\int_S \widetilde{\lambda}_p^2(\boldsymbol{N}; \overline{\mathbf{F}})\rho(\boldsymbol{N})\,\mathrm{d}S = \overline{K}_{1p}, \\ \mathbb{E}\left[\widetilde{\nu}_p^2\right] = \mathbb{E}\left[\nu_p^2\right] \quad &\Longrightarrow \quad \frac{1}{4\pi}\int_S \widetilde{\nu}_p^2(\boldsymbol{N}; \overline{\mathbf{F}})\rho(\boldsymbol{N})\,\mathrm{d}S = \overline{K}_{-1p}.\end{aligned} \tag{18}$$

By virtue of variational calculus, the resulting four Euler–Lagrange equations read

$$\frac{\partial \Psi^{0,\infty}_{\text{iso}}}{\partial \widetilde{\lambda}_p^2} = \text{const.} \qquad \text{and} \qquad \frac{\partial \Psi^{0,\infty}_{\text{iso}}}{\partial \widetilde{\nu}_p^2} = \text{const.}, \tag{19}$$

which implies optimality through

$$\begin{aligned}\widetilde{\lambda}_p^2 = \text{const.} \quad &\Longrightarrow \quad \widetilde{\lambda}_p^2 = \overline{K}_{1p}, \\ \widetilde{\nu}_p^2 = \text{const.} \quad &\Longrightarrow \quad \widetilde{\nu}_p^2 = \overline{K}_{-1p}.\end{aligned} \tag{20}$$

It is straightforward to verify that $\Psi^{0,\infty}_{\text{iso}}(\overline{K}_{\pm 1p})$ from (9) is convex in its arguments, which ensures that the extremum is a minimum. A consequence of convexity is the applicability of Jensen's inequality

$$\Psi^{0,\infty}_{\text{iso}}\left(\mathbb{E}\left[\widetilde{\lambda}_\parallel^2\right], \mathbb{E}\left[\widetilde{\nu}_\parallel^2\right], \mathbb{E}\left[\widetilde{\lambda}_\perp^2\right], \mathbb{E}\left[\widetilde{\nu}_\perp^2\right]\right) \leq \mathbb{E}\left[\Psi^{0,\infty}_{\text{iso}}(\widetilde{\lambda}_\parallel^2, \widetilde{\nu}_\parallel^2, \widetilde{\lambda}_\perp^2, \widetilde{\nu}_\perp^2)\right] \tag{21}$$

or, equivalently,

$$\Psi^{0,\infty}_{\text{iso}}(\overline{K}_{1\parallel}, \overline{K}_{-1\parallel}, \overline{K}_{1\perp}, \overline{K}_{-1\perp}) \leq \Psi^{0,\infty}_{\text{iso,avg}}\left[\widetilde{\lambda}_\parallel^2, \widetilde{\nu}_\parallel^2, \widetilde{\lambda}_\perp^2, \widetilde{\nu}_\perp^2; \overline{\mathbf{F}}\right], \tag{22}$$

which illustrates the principle of minimum averaged free energy quite tangibly.

The constrained minimization of the averaged free energy $\Psi^{0,\infty}_{\text{iso,avg}}$ can therefore be viewed as a kind of analytical homogenization of a fiber network, whereby a scale transition from a microscopic, non-affine regime to a macroscopic, affine regime is achieved.

Consequently, the introduction of structure tensors like $\mathbf{H}_{\parallel}$ and $\mathbf{H}_{\perp}$ in a free-energy function such as $\Psi_{\text{iso}}^{0,\infty}$ leads directly to a possible interpretation in terms of non-affine deformations. Notably, equivalence in (22) is attained when all fibers are aligned in a single direction, i.e. $\rho(\boldsymbol{N})$ represents a Dirac delta distribution; in this case, all microscopic and macroscopic deformation fields coincide. The whole argument is neither confined to a certain number of structure tensors nor to their respective tensor orders.

4. Stress softening

In this section, the goal is to extend the constitutive model from the previous section to include stress softening. For an overview of the experimental evidence of this phenomenon, the reader is referred to Dorfmann and Ogden (2004, sec. 2). The main observation is that some materials become more compliant after unloading and remain so when reloaded. However, if the previous load level is exceeded, the material behaves as if it had not been cycled at all until it is unloaded again. All of these concepts are first formalized in a general manner and then made explicit for a specific choice of softening function. Here we only discuss the modeling of the stiffness degradation, commonly referred to as the Mullins effect, which we will build on in the subsequent section in order to also include residual deformation, i.e. permanent set. With regard to the thermodynamics of modeling the Mullins effect, the authors highly recommend (Naumann and Ihlemann, 2015).

4.1. Thermodynamic framework

In order to model the switch from the primary loading path to the unloading and reloading path, an internal variable is introduced that tracks the evolution of the maximally attained 'undamaged' isochoric free energy, i.e.

$$\Psi_{\text{iso}}^{\max}(t) = \max_{\tau \le t} \Psi_{\text{iso}}^{0,\infty}(\tau), \tag{23}$$

cf. Naumann and Ihlemann (2015, eq. 8). From here, we refer to the time intervals between updates of $\Psi_{\text{iso}}^{\max}$ as unloading–reloading cycles. Although the time t is explicitly mentioned, the model remains rate-independent.

We can now define a softening function $\eta_{\text{m}}(\Psi_{\text{iso}}^{0,\infty}, \Psi_{\text{iso}}^{\max})$ that scales the stress response in (14) depending on whether the material is currently experiencing primary loading or not, such that

$$\mathbf{S} = J^{-2/3}\mathbb{P} : \left(\eta_{\text{m}}\overline{\mathbf{S}}^{0,\infty}\right) + \mathbf{S}_{\text{vol}}^{0,\infty}. \tag{24}$$

For physical reasons, $0 < \eta_{\text{m}} \le 1$ with $\eta_{\text{m}}(\Psi_{\text{iso}}^{\max}, \Psi_{\text{iso}}^{\max}) = 1$. Once more we emphasize that the inelastic effects act only on the isochoric stress response. The superscript/subscript 'm' refers to quantities related to the Mullins effect.

According to Naumann and Ihlemann (2015, eq. 28), the corresponding 'damaged' isochoric free-energy function is defined as

$$\Psi_{\text{iso}}^{\text{m},\infty}(\overline{\mathbf{C}}, \Psi_{\text{iso}}^{\max}) = \int_0^t \eta_{\text{m}}\left[\Psi_{\text{iso}}^{0,\infty}(\tau), \Psi_{\text{iso}}^{\max}(t)\right] \dot{\Psi}_{\text{iso}}^{0,\infty}(\tau)\,\mathrm{d}\tau = \int_0^{\Psi_{\text{iso}}^{0,\infty}} \eta_{\text{m}}(\psi, \Psi_{\text{iso}}^{\max})\,\mathrm{d}\psi. \tag{25}$$

Whether or not the time differentiation is evaluated at t or τ should be clear from the context or is stated explicitly with parentheses to avoid ambiguity. In the last step, the substitution $\mathrm{d}\Psi_{\text{iso}}^{0,\infty} = \dot{\Psi}_{\text{iso}}^{0,\infty}(\tau)\,\mathrm{d}\tau$ is used and ψ serves as a dummy variable to avoid confusion with the upper limit of integration.

Keeping the Leipniz integral rule in mind, the derivative of (25) with respect to t yields

$$\begin{aligned}\dot{\Psi}_{\text{iso}}^{\text{m},\infty} &= \int_0^{\Psi_{\text{iso}}^{0,\infty}} \frac{\partial \eta_{\text{m}}}{\partial \Psi_{\text{iso}}^{\max}}\,\mathrm{d}\psi\,\dot{\Psi}_{\text{iso}}^{\max} + \eta_{\text{m}}(\Psi_{\text{iso}}^{0,\infty}, \Psi_{\text{iso}}^{\max})\dot{\Psi}_{\text{iso}}^{0,\infty} \\ &= \int_0^{\Psi_{\text{iso}}^{0,\infty}} \frac{\partial \eta_{\text{m}}}{\partial \Psi_{\text{iso}}^{\max}}\,\mathrm{d}\psi\,\dot{\Psi}_{\text{iso}}^{\max} + \frac{1}{2}\eta_{\text{m}}\overline{\mathbf{S}}^{0,\infty} : \dot{\overline{\mathbf{C}}}.\end{aligned} \tag{26}$$

If we insert $\Psi_{\text{iso}}^{\text{m},\infty}$ into (4), we can again bracket the terms with $\dot{\mathbf{C}}$, whereupon we recover (24); the reduced Mullins-related dissipation reads

$$\mathcal{D}_{\text{m}} = -\int_0^{\Psi_{\text{iso}}^{0,\infty}} \frac{\partial \eta_{\text{m}}}{\partial \Psi_{\text{iso}}^{\max}}\,\mathrm{d}\psi\,\dot{\Psi}_{\text{iso}}^{\max} = -\int_0^{\Psi_{\text{iso}}^{\max}} \frac{\partial \eta_{\text{m}}}{\partial \Psi_{\text{iso}}^{\max}}\,\mathrm{d}\psi\,\dot{\Psi}_{\text{iso}}^{\max} \ge 0. \tag{27}$$

By definition, $\dot{\Psi}_{\text{iso}}^{\max} \ge 0$ and therefore dissipation only occurs during primary loading, where $\Psi_{\text{iso}}^{0,\infty} = \Psi_{\text{iso}}^{\max} \ge 0$, which explains the change in the upper limit of integration. As stated in Naumann and Ihlemann (2015, eq. 37), the sufficient condition

$$\frac{\partial \eta_{\text{m}}}{\partial \Psi_{\text{iso}}^{\max}} \le 0 \tag{28}$$

ensures (27).

Remark 5. The integration by substitution in (25) skips over the detail that $\Psi_{\text{iso}}^{0,\infty}(t)$ is not injective, i.e. two different points in time $t_1 \neq t_2$ might correspond to the same energy function $\Psi_{\text{iso}}^{0,\infty}(t_1) = \Psi_{\text{iso}}^{0,\infty}(t_2)$. Only due to the potential character of $\Psi_{\text{iso}}^{\text{m},\infty}$, a more thorough treatment is unnecessary.

Remark 6. Here, a thermodynamic discussion of the formulation (25) reveals a requirement for $\eta_{\text{m}}(\Psi_{\text{iso}}^{0,\infty}, \Psi_{\text{iso}}^{\max})$. Interestingly, the choices made by Ogden and Roxburgh (1999, eq. 3.28) and Dorfmann and Ogden (2004, eq. 57) conform to (28) without this thermodynamic reasoning, but another more heuristic argument, cf. Ogden and Roxburgh (1999, eq. 3.16).

4.2. Specific choice of softening function

In order to align the modeling of stress softening and permanent set in a more streamlined manner, we introduce the auxiliary function

$$\eta(\chi;\eta_0,\eta_1,\alpha)=\eta_0+(\eta_1-\eta_0)\big[(\alpha+1)\chi^{\alpha}-\alpha\chi^{\alpha+1}\big]\qquad\text{with}\qquad\chi=\frac{\Psi_{\mathrm{iso}}^{0,\infty}}{\Psi_{\mathrm{iso}}^{\max}}\tag{29}$$

and $\alpha\geq 1$. Note that $0\leq\chi\leq 1$. The domain of (29) is then confined by $\eta(0)=\eta_0$ and $\eta(1)=\eta_1$. Also note that the derivative η' is monotonic with respect to χ, in particular $\eta'(1)=0$, leading to continuous gradients in the stress response.

In the case of Mullins-related stiffness loss, we specify (29) to

$$\eta_{\mathrm{m}}(\Psi_{\mathrm{iso}}^{0,\infty},\Psi_{\mathrm{iso}}^{\max})=\eta\big(\chi;\eta_{\mathrm{m0}},1,\alpha_{\mathrm{m}}\big)=\eta_{\mathrm{m0}}+(1-\eta_{\mathrm{m0}})\big[(\alpha_{\mathrm{m}}+1)\chi^{\alpha_{\mathrm{m}}}-\alpha_{\mathrm{m}}\chi^{\alpha_{\mathrm{m}}+1}\big],\tag{30}$$

where $0<\eta_{\mathrm{m0}}\leq 1$. As physically required, the softening function leaves the stress response (24) unchanged on the primary loading path, where $\chi=1$ and $\eta_{\mathrm{m}}(1)=1$, and scales it to a value $\eta_{\mathrm{m0}}\leq\eta_{\mathrm{m}}(\chi)<1$ during unloading and reloading, where $\chi<1$. For illustration, Fig. 3(a),(c) show three example trajectories of (30) for different parameter choices $\theta_{\mathrm{m},\infty}=(\eta_{\mathrm{m0}},\alpha_{\mathrm{m}})$.

By routine differentiation, it can be checked that (30) conforms to (28) and by integration of (27) we get the closed-form expression

$$\begin{aligned}D_{\mathrm{m}}&=\frac{(1-\eta_{\mathrm{m0}})\alpha_{\mathrm{m}}(\alpha_{\mathrm{m}}+1)}{\Psi_{\mathrm{iso}}^{\max}}\int_0^{\Psi_{\mathrm{iso}}^{\max}}\chi^{\alpha_{\mathrm{m}}}(1-\chi)\,\mathrm{d}\psi\,\dot{\Psi}_{\mathrm{iso}}^{\max}\\&=(1-\eta_{\mathrm{m0}})\frac{\alpha_{\mathrm{m}}}{\alpha_{\mathrm{m}}+2}\dot{\Psi}_{\mathrm{iso}}^{\max}\geq 0.\end{aligned}\tag{31}$$

With the aforementioned restrictions on η_{m0} and α_{m}, the inequality holds in general.

Likewise, the 'damaged' isochoric free-energy function in (25) can be integrated analytically, which leads to

$$\begin{aligned}\Psi_{\mathrm{iso}}^{\mathrm{m},\infty}(\Psi_{\mathrm{iso}}^{0,\infty},\Psi_{\mathrm{iso}}^{\max})&=\int_0^{\Psi_{\mathrm{iso}}^{0,\infty}}\eta_{\mathrm{m0}}+(1-\eta_{\mathrm{m0}})\big[(\alpha_{\mathrm{m}}+1)\chi_{\mathrm{m}}^{\alpha}-\alpha_{\mathrm{m}}\chi^{\alpha_{\mathrm{m}}+1}\big]\,\mathrm{d}\psi\\&=\left[\eta_{\mathrm{m0}}+(1-\eta_{\mathrm{m0}})\left(\chi^{\alpha_{\mathrm{m}}}-\frac{\alpha_{\mathrm{m}}}{\alpha_{\mathrm{m}}+2}\chi^{\alpha_{\mathrm{m}}+1}\right)\right]\Psi_{\mathrm{iso}}^{0,\infty}.\end{aligned}\tag{32}$$

For the special case $\eta_{\mathrm{m0}}=1$, the softening function $\eta_{\mathrm{m}}(\chi)\equiv 1$, i.e. no stress softening ever occurs, and $\Psi_{\mathrm{iso}}^{\mathrm{m},\infty}\equiv\Psi_{\mathrm{iso}}^{0,\infty}$.

In Fig. 3(b),(d), the influence of the Mullins-related material parameters for cyclic, uniaxial extension is illustrated. Now, there are a total of ten material constants consisting of $\theta_{0,\infty}=(H_1,H_2,\mu_{\parallel},\mu_{\perp},\gamma_{\parallel},\gamma_{\perp},\delta_{\parallel},\delta_{\perp})$ and $\theta_{\mathrm{m},\infty}=(\eta_{\mathrm{m0}},\alpha_{\mathrm{m}})$. Evidently, η_{m0} determines the magnitude of the damage, while the shape parameter α_{m} governs the evolution of stress softening during unloading.

Remark 7. Interestingly, the thermodynamic argument does not provide a lower bound for η_{m0}, although for physical reasons $\eta_{\mathrm{m0}}>0$, otherwise we would acquire a negative semi-definite stiffness tensor and conversely obtain negative energies as evidenced by (32).

Remark 8. In general, a consequence of using the ratio χ when modeling η_{m} is the lack of dependence of D_{m} on $\Psi_{\mathrm{iso}}^{\max}$, i.e. the accumulated dissipation is always linear in $\Psi_{\mathrm{iso}}^{\max}$; this can be checked with the substitution $\mathrm{d}\psi=\Psi_{\mathrm{iso}}^{\max}\,\mathrm{d}\chi$ in (27) reading

$$\mathcal{D}_{\mathrm{m}}=-\int_0^{\Psi_{\mathrm{iso}}^{\max}}\frac{\partial\eta_{\mathrm{m}}}{\partial\Psi_{\mathrm{iso}}^{\max}}\,\mathrm{d}\psi\,\dot{\Psi}_{\mathrm{iso}}^{\max}=\int_0^{\Psi_{\mathrm{iso}}^{\max}}\frac{\partial\eta_{\mathrm{m}}}{\partial\chi}\frac{\chi}{\Psi_{\mathrm{iso}}^{\max}}\,\mathrm{d}\psi\,\dot{\Psi}_{\mathrm{iso}}^{\max}=\int_0^1\frac{\partial\eta_{\mathrm{m}}}{\partial\chi}\chi\,\mathrm{d}\chi\,\dot{\Psi}_{\mathrm{iso}}^{\max},\tag{33}$$

which is independent from $\Psi_{\mathrm{iso}}^{\max}$ as claimed. A nonlinear behavior can be allowed, e.g., by working with the difference $\Psi_{\mathrm{iso}}^{\max}-\Psi_{\mathrm{iso}}^{0,\infty}\geq 0$, which then also necessitates the introduction of an energy-like material parameter.

5. Permanent set

Here we extend the above framework to model stress softening, now including residual deformation. In the current state of the constitutive model, the material might display damage after unloading, which is noticeable as a loss of stiffness, but the material remains elastic thereafter, cf. Naumann and Ihlemann (2015, rem. 1). We can therefore not capture any inelastic deformation that may occur, see, e.g., Dorfmann and Ogden (2004, fig. 1). Although many concepts from the modeling of the stiffness degradation carry over, to the best of the authors' knowledge, the consequences of using the pseudo-elastic formulation for permanent set, originally proposed by Dorfmann and Ogden (2004), have not been discussed in a general manner so far. To this end, we again first formalize the necessary concepts and attempt to investigate them in a formal analysis. We then choose a specific formulation and illustrate the resulting constitutive predictions.

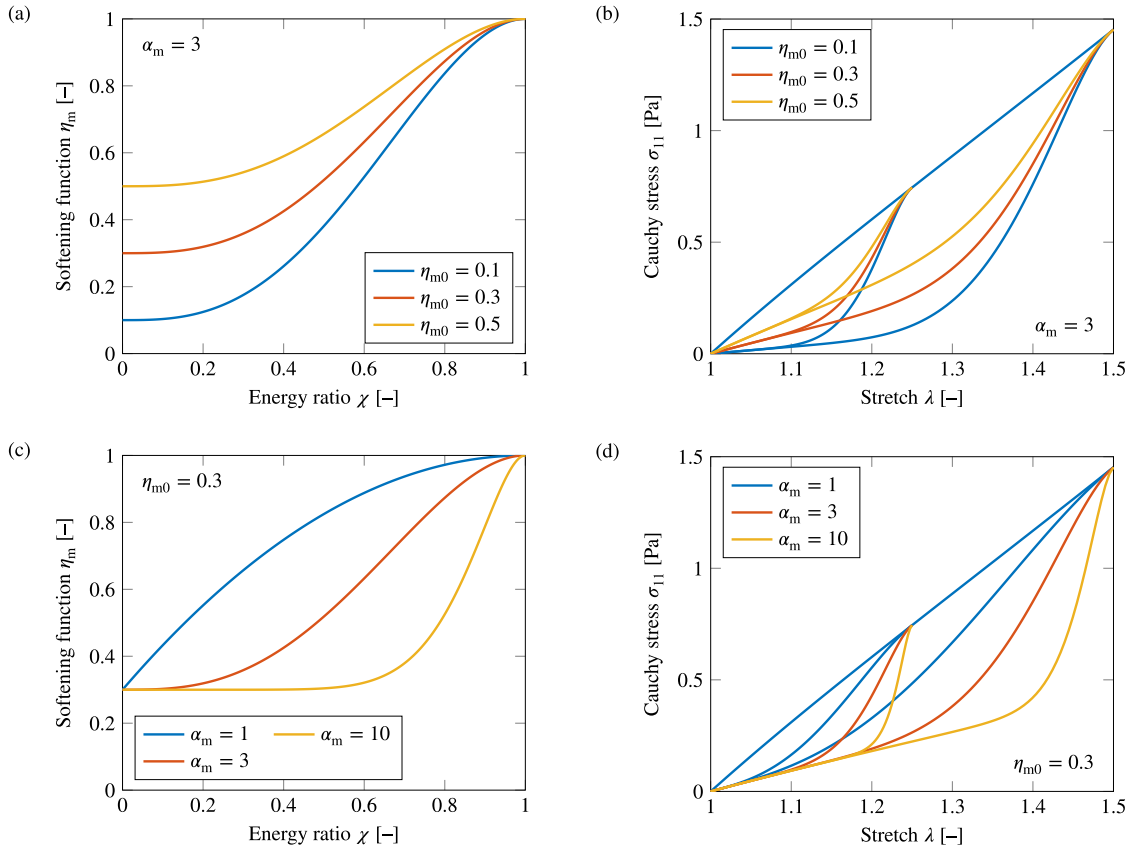

Fig. 3. Three examples for (a) the trajectory of the Mullins-related softening function for constant α_m and changing η_{m0} and (b) the quasi-static, cyclic, uniaxial stress response given the softening functions from (a). Analogously, three examples for (c) the trajectory of the Mullins-related softening function for constant η_{m0} and changing α_m and (d) the quasi-static, cyclic, uniaxial stress response given the softening functions from (c). The 'undamaged' parameters are kept constant with $\theta_{0,\infty} = (0.7, 0.3, 1\,\text{Pa}, 0.2\,\text{Pa}, 0, 0, 0, 0)$.

5.1. Residual stress contribution

Both in Dorfmann and Ogden (2004, eqs. 49, 67, 72) and Fereidoonnezhad et al. (2016, eqs. 10, 20) the basic idea to include permanent set is through the introduction of an inelastic, residual stress tensor $\overline{\mathbf{S}}^{\mathrm{r},\infty}(\overline{\mathbf{C}}^{\star})$, which depends on the isochoric deformation state $\overline{\mathbf{C}}^{\star}$ at the instance of the maximally attained isochoric free energy $\Psi_{\mathrm{iso}}^{\max}$, i.e.

$$\overline{\mathbf{C}}^{\star}(t) = \overline{\mathbf{C}}(\tau^{\star}) \qquad \text{with} \qquad \tau^{\star} = \operatorname*{arg\,max}_{\tau \le t} \Psi_{\mathrm{iso}}^{0,\infty}(\tau) \qquad \Longrightarrow \qquad \Psi_{\mathrm{iso}}^{\max} = \Psi_{\mathrm{iso}}^{0,\infty}(\overline{\mathbf{C}}^{\star}). \tag{34}$$

The additional stress contribution is then switched on and off continuously with a softening function $\eta_{\mathrm{r}}(\Psi_{\mathrm{iso}}^{0,\infty}, \Psi_{\mathrm{iso}}^{\max})$, similar to $\eta_{\mathrm{m}}(\Psi_{\mathrm{iso}}^{0,\infty}, \Psi_{\mathrm{iso}}^{\max})$ from (24), which leads to the quasi-static stress formulation

$$\mathbf{S} = J^{-2/3}\mathbb{P} : \overline{\mathbf{S}}^{\infty} + \mathbf{S}_{\mathrm{vol}}^{0,\infty} = J^{-2/3}\mathbb{P} : \left(\eta_{\mathrm{m}}\overline{\mathbf{S}}^{0,\infty} + \eta_{\mathrm{r}}\overline{\mathbf{S}}^{\mathrm{r},\infty}\right) + \mathbf{S}_{\mathrm{vol}}^{0,\infty}. \tag{35}$$

Here, the superscript/subscript 'r' denotes the terms associated with permanent set. Since $\overline{\mathbf{S}}^{\mathrm{r},\infty}$ should not affect the material behavior during primary loading, $\eta_{\mathrm{r}}(\Psi_{\mathrm{iso}}^{\max}, \Psi_{\mathrm{iso}}^{\max}) = 0$. We note that our definition of η_{r} differs slightly from the original publications.

For general deformations, choosing a relation $\overline{\mathbf{S}}^{\mathrm{r},\infty}(\overline{\mathbf{C}}^{\star})$ that leads to consistent physical residual stress responses is challenging. This difficulty arises because there does not seem to be a thermodynamic framework for treating permanent set, unlike for stress softening, which is discussed in Section 4.1.

Before continuing, we briefly introduce the set of all isochoric deformation states with free energy (less than or) equal to $\Psi_{\mathrm{iso}}^{\max}$, i.e.

$$\mathcal{S}_{\mathrm{eq}} = \{\overline{\mathbf{C}} \mid \Psi_{\mathrm{iso}}^{0,\infty}(\overline{\mathbf{C}}) = \Psi_{\mathrm{iso}}^{\max}\} \qquad \text{and} \qquad \mathcal{S}_{\mathrm{leq}} = \{\overline{\mathbf{C}} \mid \Psi_{\mathrm{iso}}^{0,\infty}(\overline{\mathbf{C}}) \le \Psi_{\mathrm{iso}}^{\max}\}. \tag{36}$$

Remark 9. There is a slight ambiguity in the definition of $\overline{\mathbf{C}}^\star$ given by (34) in the limit case when $\Psi_{\text{iso}}^{0,\infty}$ reaches $\Psi_{\text{iso}}^{\max}$ after reloading, but for a different deformation than the current $\overline{\mathbf{C}}^\star$, upon which no further primary loading follows. In order to resolve this indeterminacy, we decide to update $\overline{\mathbf{C}}^\star$ only after a 'new' maximum in $\Psi_{\text{iso}}^{0,\infty}$ is reached.

5.2. Net work in a cycle

Given the stress formulation in (35), it is not self-evident how a proper thermodynamic argument should be constructed that reveals requirements about the constitutive modeling of η_{r} and $\overline{\mathbf{S}}^{\text{r},\infty}$ in a physically meaningful way. Hence, we turn to a more tangible constitutive inequality, given by Hill (1968, p. 232), which requires the net work done by strain cycles, i.e. 'paths of deformation that begin and end in the same configuration', to be non-negative. We slightly modify this requirement and ask about the net work done in an unloading–reloading cycle instead. For us, 'same configuration' is thus defined as all $\overline{\mathbf{C}} \in \mathcal{S}_{\text{eq}}$. Although an interesting concept in its own right, it will later also be relevant for attempting to define a meaningful free-energy function associated with permanent set.

With (35), Hill's strain cycle condition reads

$$\begin{aligned} w_{\text{cycle}} &= \frac{1}{2}\oint \mathbf{S} : \dot{\mathbf{C}}\,\mathrm{d}\tau = \frac{1}{2}\oint \left[\left(\eta_{\text{m}}\overline{\mathbf{S}}^{0,\infty} + \eta_{\text{r}}\overline{\mathbf{S}}^{\text{r},\infty}\right) : \dot{\overline{\mathbf{C}}} + \mathbf{S}_{\text{vol}}^{0,\infty} : \dot{\mathbf{C}}\right]\mathrm{d}\tau \\ &= \frac{1}{2}\oint \eta_{\text{r}}\overline{\mathbf{S}}^{\text{r},\infty} : \dot{\overline{\mathbf{C}}}\,\mathrm{d}\tau \geq 0, \end{aligned} \tag{37}$$

where the integral over the volumetric and Mullins-related terms vanishes due to their conservative nature and only the η_{r}-weighted residual power (density) remains of relevance.

For a residual stress formulation of the form (35), it can be shown that the requirement (37) is generally not fulfilled. We do this by proof of contraction. Let us assume that the condition (37) holds in general; then it also holds for any path of isochoric deformation $\overline{\mathbf{C}}(\tau)$ during an unloading–reloading cycle that starts and ends in the same deformation state, i.e. $t_a \leq \tau \leq t_b$ with $\overline{\mathbf{C}}(t_a) = \overline{\mathbf{C}}(t_b) = \overline{\mathbf{C}}^\star$ and $\Psi_{\text{iso}}^{0,\infty}[\overline{\mathbf{C}}(\tau)] \leq \Psi_{\text{iso}}^{\max}$. By definition, $\Psi_{\text{iso}}^{\max} = \text{const.}$ and consequently $\overline{S}_{IJ}^{\text{r},\infty} = \text{const.}$ From (37), we get

$$w_{\text{cycle}} = \frac{1}{2}\int_{t_a}^{t_b} \eta_{\text{r}}\overline{\mathbf{S}}^{\text{r},\infty} : \dot{\overline{\mathbf{C}}}\,\mathrm{d}\tau = \frac{1}{2}\overline{\mathbf{S}}^{\text{r},\infty} : \int_{t_a}^{t_b} \eta_{\text{r}}[\overline{\mathbf{C}}(\tau)]\dot{\overline{\mathbf{C}}}(\tau)\,\mathrm{d}\tau. \tag{38}$$

Let us now traverse this closed path of deformation in the reverse sense, so that $\tau' = t_b - (\tau - t_a)$ and $\overline{\mathbf{C}}'(\tau) = \overline{\mathbf{C}}(\tau')$, which is itself a valid closed path of deformation. Then,

$$w'_{\text{cycle}} = -w_{\text{cycle}} \quad \Longrightarrow \quad w'_{\text{cycle}} \leq 0. \tag{39}$$

In the absence of a potential, we can always find a path of deformation for which the work is non-zero and therefore either itself or its reverse counterpart contradicts the assumption (37), which then cannot hold in general for the modeling approach presented in (35). In fact, one can show that there exist unloading–reloading cycles for which the net work, be it positive or negative, is unbounded, see Appendix A. This also renders a variational treatment of (38) difficult, since there might not exist global optima which could be used to establish bounds on w_{cycle}. Whether or not these types of deformation paths are relevant to application is another question, though.

Although we have established that given (35) we can always construct an unphysical unloading–reloading cycle, we do not want to deem the approach inappropriate *per se*. There is a reasonable choice for $\overline{\mathbf{S}}^{\text{r},\infty}$ that suggests a positive net work in an averaged sense, as shown below.

5.3. Specific choice for the residual stress formulation

We define the residual stress contribution in the form

$$\overline{\mathbf{S}}^{\text{r},\infty}(\overline{\mathbf{C}}^\star) = -\overline{\mathbf{S}}^{0,\infty}(\overline{\mathbf{C}}^\star). \tag{40}$$

Somewhat intuitively, the residual stresses 'counteract' the stress state encountered at $\overline{\mathbf{C}}^\star$. More importantly, there is a mathematical advantage. We can use the convexity of (9) with respect to $\overline{\mathbf{C}}$. The proof thereof can be found in Appendix B. As $\Psi_{\text{iso}}^{0,\infty}$ is sufficiently smooth,

$$\Psi_{\text{iso}}^{0,\infty}(\overline{\mathbf{C}}) - \Psi_{\text{iso}}^{0,\infty}(\overline{\mathbf{C}}^\star) - \frac{1}{2}\overline{\mathbf{S}}^{0,\infty}(\overline{\mathbf{C}}^\star) : \left(\overline{\mathbf{C}} - \overline{\mathbf{C}}^\star\right) \geq 0 \quad \forall \overline{\mathbf{C}}, \overline{\mathbf{C}}^\star, \tag{41}$$

cf. Ogden (1997, eq. A.8). Since $\Psi_{\text{iso}}^{0,\infty}(\overline{\mathbf{C}}^\star) = \Psi_{\text{iso}}^{\max}$, it follows with (40) that

$$\frac{1}{2}\overline{\mathbf{S}}^{\text{r},\infty} : \left(\overline{\mathbf{C}} - \overline{\mathbf{C}}^\star\right) \geq \Psi_{\text{iso}}^{\max} - \Psi_{\text{iso}}^{0,\infty} \geq 0 \quad \forall \overline{\mathbf{C}} \in \mathcal{S}_{\text{leq}}. \tag{42}$$

Ultimately, we are interested in a kind of expected value for the net work w_{cycle} in a finite unloading–reloading cycle, which is not straightforward to define, since the sample space of all deformation paths $\overline{\mathbf{C}}(\tau)$ is unaccountably infinite. If one interprets

the deformation path during an unloading–reloading cycle as a stochastic process, (37) can be rewritten in the form of a Fisk–Stratonovich integral

$$w_{\text{cycle}} = \frac{1}{2}\int_{t_a}^{t_b} \eta_{\text{r}}\overline{\mathbf{S}}^{\text{r},\infty} : \dot{\overline{\mathbf{C}}}\,\mathrm{d}\tau = \lim_{\Delta t\to 0}\frac{1}{2}\sum_{i=0}^{N-1}\frac{\eta_{\text{r}}(\overline{\mathbf{C}}_{i+1})+\eta_{\text{r}}(\overline{\mathbf{C}}_i)}{2}\overline{\mathbf{S}}^{\text{r},\infty} : \left(\overline{\mathbf{C}}_{i+1}-\overline{\mathbf{C}}_i\right), \tag{43}$$

where $\overline{\mathbf{C}}_i = \overline{\mathbf{C}}(t_i)$ and $t_a = t_0 < t_1 < \cdots < t_{N-1} < t_N = t_b$ with $\Delta t = (t_b - t_a)/(N+1)$, cf. Fisk (1963, sec. 2.2.1). By definition, $\eta_{\text{r}}(\overline{\mathbf{C}}_0) = \eta_{\text{r}}(\overline{\mathbf{C}}_N) = 0$ and (43) reduces to

$$\begin{aligned} w_{\text{cycle}} &= \lim_{\Delta t\to 0}\frac{1}{4}\overline{\mathbf{S}}^{\text{r},\infty} : \left[\sum_{i=1}^{N-1}\eta_{\text{r}}(\overline{\mathbf{C}}_i)\overline{\mathbf{C}}_{i+1} - \sum_{i=0}^{N-2}\eta_{\text{r}}(\overline{\mathbf{C}}_{i+1})\overline{\mathbf{C}}_i\right] \\ &= \lim_{\Delta t\to 0}\frac{1}{4}\overline{\mathbf{S}}^{\text{r},\infty} : \left[\eta_{\text{r}}(\overline{\mathbf{C}}_{N-1})\overline{\mathbf{C}}_N - \eta_{\text{r}}(\overline{\mathbf{C}}_1)\overline{\mathbf{C}}_0 + \sum_{i=1}^{N-2}\eta_{\text{r}}(\overline{\mathbf{C}}_i)\overline{\mathbf{C}}_{i+1} - \eta_{\text{r}}(\overline{\mathbf{C}}_{i+1})\overline{\mathbf{C}}_i\right]. \end{aligned} \tag{44}$$

Any unloading–reloading cycle must start at $\overline{\mathbf{C}}_0 = \overline{\mathbf{C}}^\star$ and end at some $\overline{\mathbf{C}}_N = \overline{\mathbf{C}} \in \mathcal{S}_{\text{eq}}$, but during the unloading–reloading cycle, i.e. $i \notin \{0, N\}$, all deformation states in $\mathcal{S}_{\text{leq}}$ are equally likely. Therefore, similar to a path integral, we define the expected value for the net work as

$$\mathbb{E}\left[w_{\text{cycle}}\right] = \frac{1}{Z^{N-1}}\int\cdots\int w_{\text{cycle}}\,\mathrm{d}\overline{\mathbf{C}}_1\ldots\mathrm{d}\overline{\mathbf{C}}_{N-1} \tag{45}$$

with

$$Z^{N-1} = \int\cdots\int \mathrm{d}\overline{\mathbf{C}}_1\ldots\mathrm{d}\overline{\mathbf{C}}_{N-1} = \left(\int \mathrm{d}\overline{\mathbf{C}}_i\right)^{N-1}, \tag{46}$$

i.e. $Z = \int \mathrm{d}\overline{\mathbf{C}}_i$ for all $i \notin \{0, N\}$. The integrals over the five independent entries in each $\overline{\mathbf{C}}_i \in \mathcal{S}_{\text{leq}}$ are well defined, since $\mathcal{S}_{\text{leq}}$ is a closed set. If we define

$$\mathbb{E}\left[\overline{\mathbf{C}}\right] = \frac{1}{Z}\int \overline{\mathbf{C}}_i\,\mathrm{d}\overline{\mathbf{C}}_i \qquad \text{and} \qquad \mathbb{E}\left[\eta_{\text{r}}\right] = \frac{1}{Z}\int \eta_{\text{r}}(\overline{\mathbf{C}}_i)\,\mathrm{d}\overline{\mathbf{C}}_i \tag{47}$$

for all $i \notin \{0, N\}$, we can simplify (45) with (43) considerably through

$$\begin{aligned} \mathbb{E}\left[w_{\text{cycle}}\right] &= \lim_{\Delta t\to 0}\frac{1}{4}\overline{\mathbf{S}}^{\text{r},\infty} : \left\{\frac{1}{Z^{N-1}}\int\cdots\int\left[\eta_{\text{r}}(\overline{\mathbf{C}}_{N-1})\overline{\mathbf{C}}_N - \eta_{\text{r}}(\overline{\mathbf{C}}_1)\overline{\mathbf{C}}_0 + \sum_{i=1}^{N-2}\eta_{\text{r}}(\overline{\mathbf{C}}_i)\overline{\mathbf{C}}_{i+1} - \eta_{\text{r}}(\overline{\mathbf{C}}_{i+1})\overline{\mathbf{C}}_i\right]\mathrm{d}\overline{\mathbf{C}}_1\ldots\mathrm{d}\overline{\mathbf{C}}_{N-1}\right\} \\ &= \lim_{\Delta t\to 0}\frac{1}{4}\overline{\mathbf{S}}^{\text{r},\infty} : \left(\mathbb{E}\left[\eta_{\text{r}}\right]\overline{\mathbf{C}}_N - \mathbb{E}\left[\eta_{\text{r}}\right]\overline{\mathbf{C}}_0 + \sum_{i=1}^{N-2}\mathbb{E}\left[\eta_{\text{r}}\right]\mathbb{E}\left[\overline{\mathbf{C}}\right] - \mathbb{E}\left[\eta_{\text{r}}\right]\mathbb{E}\left[\overline{\mathbf{C}}\right]\right) \\ &= \frac{1}{4}\mathbb{E}\left[\eta_{\text{r}}\right]\overline{\mathbf{S}}^{\text{r},\infty} : \left(\overline{\mathbf{C}} - \overline{\mathbf{C}}^\star\right) \quad \forall\overline{\mathbf{C}} \in \mathcal{S}_{\text{eq}}. \end{aligned} \tag{48}$$

It follows that for $\mathbb{E}\left[w_{\text{cycle}}\right]$ to be non-negative, we require that $\mathbb{E}\left[\eta_{\text{r}}\right]$ and $\overline{\mathbf{S}}^{\text{r},\infty} : (\overline{\mathbf{C}} - \overline{\mathbf{C}}^\star)$ have the same sign. For the latter we already know from (42) that

$$\frac{1}{2}\overline{\mathbf{S}}^{\text{r},\infty} : \left(\overline{\mathbf{C}} - \overline{\mathbf{C}}^\star\right) \geq 0 \quad \forall\overline{\mathbf{C}} \in \mathcal{S}_{\text{eq}} \quad \Longleftarrow \quad \mathcal{S}_{\text{eq}} \subset \mathcal{S}_{\text{leq}}. \tag{49}$$

Hence, we are left with the requirement $\mathbb{E}\left[\eta_{\text{r}}\right] \geq 0$ which is sufficiently satisfied through

$$\eta_{\text{r}}(\Psi_{\text{iso}}^{0,\infty}, \Psi_{\text{iso}}^{\max}) \geq 0. \tag{50}$$

Therefore, given the residual stress formulation (40), we can show that for a random deformation path the expected value for the net work in an unloading–reloading cycle is non-negative, if (50) holds.

With the consequences of Hill's strain cycle condition at hand, it is possible to carry over the results in an attempt to define a free-energy function $\Psi_{\text{iso}}^{\text{r},\infty}$ related to permanent set in the form

$$\Psi_{\text{iso}}^{\text{r},\infty}(\overline{\mathbf{C}}, \overline{\mathbf{C}}^\star) = \frac{1}{2}\eta_{\text{r}}(\Psi_{\text{iso}}^{0,\infty}, \Psi_{\text{iso}}^{\max})\overline{\mathbf{S}}^{\text{r},\infty}(\overline{\mathbf{C}}^\star) : \left(\overline{\mathbf{C}} - \overline{\mathbf{C}}^\star\right). \tag{51}$$

To avoid possible limiting issues in the initial, undeformed configuration, we set $\eta_{\text{r}}(0, 0) = 0$. With (42) and (50) it is straightforward to check that $\Psi_{\text{iso}}^{\text{r},\infty} \geq 0$. If we take $\Psi_{\text{iso}}^{\infty} = \Psi_{\text{iso}}^{\text{m},\infty} + \Psi_{\text{iso}}^{\text{r},\infty}$ and plug it into (4), we can bracket the terms with $\dot{\overline{\mathbf{C}}}$ as usual resulting in (35), as desired. The reduced dissipation associated with permanent set reads

$$\begin{aligned} D_{\text{r}} &= -\frac{1}{2}\dot{\eta}_{\text{r}}\overline{\mathbf{S}}^{\text{r},\infty} : \left(\overline{\mathbf{C}} - \overline{\mathbf{C}}^\star\right) + \frac{1}{2}\eta_{\text{r}}\left(\overline{\mathbf{S}}^{\text{r},\infty} : \overline{\mathbf{C}}^\star\right)^{\cdot} \\ &= -\frac{1}{2}\dot{\eta}_{\text{r}}\overline{\mathbf{S}}^{\text{r},\infty} : \left(\overline{\mathbf{C}} - \overline{\mathbf{C}}^\star\right) \geq 0, \end{aligned} \tag{52}$$

where the second term on the right-hand side vanishes, since either η_{r} or $\dot{\overline{\mathbf{C}}}^\star$ is zero at all times. Because of instances with $\dot{\eta}_{\text{r}} > 0$, the dissipation inequality does not hold in general. However, if we look at the accumulated dissipation and notice that $\dot{\eta}_{\text{r}} = 0$ during

primary loading, then

$$\begin{aligned}\int_0^{\tau^\star} \mathcal{D}_\mathrm{r}\,\mathrm{d}\tau &= -\frac{1}{2}\int_0^{\tau^\star} \dot{\eta}_\mathrm{r}\,\overline{\mathbf{S}}^{\mathrm{r},\infty} : \left(\overline{\mathbf{C}} - \overline{\mathbf{C}}^\star\right)\mathrm{d}\tau \\ &= \sum_{\text{cycles}} -\frac{1}{2}\oint \dot{\eta}_\mathrm{r}\,\overline{\mathbf{S}}^{\mathrm{r},\infty} : \left(\overline{\mathbf{C}} - \overline{\mathbf{C}}^\star\right)\mathrm{d}\tau \\ &= \sum_{\text{cycles}} \frac{1}{2}\oint \eta_\mathrm{r}\,\overline{\mathbf{S}}^{\mathrm{r},\infty} : \dot{\overline{\mathbf{C}}}\,\mathrm{d}\tau \\ &= \sum_{\text{cycles}} w_{\text{cycle}},\end{aligned} \tag{53}$$

where in the second step each unloading–reloading cycle is rewritten by partial integration. For more details about this operation, the reader is referred to (A.2). From the results obtained so far, it follows directly that also the expected accumulated dissipation up to $\tau^\star$ is non-negative for a random deformation path in the sense given above.

Taking into account (50), we again use (29) from Section 4.2 and define

$$\begin{aligned}\eta_\mathrm{r}(\Psi_{\text{iso}}^{0,\infty}, \Psi_{\text{iso}}^{\max}) &= \eta\big(\chi; \eta_{\mathrm{r}0}, 0, \alpha_\mathrm{r}\big) \\ &= \eta_{\mathrm{r}0}\left[1 - (\alpha_\mathrm{r}+1)\chi^{\alpha_\mathrm{r}} + \alpha_\mathrm{r}\chi^{\alpha_\mathrm{r}+1}\right] \qquad \text{with} \qquad \chi = \frac{\Psi_{\text{iso}}^{0,\infty}}{\Psi_{\text{iso}}^{\max}},\end{aligned} \tag{54}$$

which inherits the advantages pointed out in the discussion on the modeling of stress softening.

The Fig. 4(a),(c) show three examples of (54) for different parameter choices $\theta_{\mathrm{r},\infty} = (\eta_{\mathrm{r}0}, \alpha_\mathrm{r})$, which adds two additional material parameters to the constitutive model, now a total of twelve. In Fig. 4(b),(d), the stress response to the same cyclic, uniaxial boundary-value problem, as discussed in Section 4.2, is plotted, but now including permanent set. It is evident that the material does not return to a stress-free initial configuration and that the choice of $\eta_{\mathrm{r}0}$ controls the magnitude of the residual stress contribution, while the shape parameter α_r governs its evolution during unloading. We note that the residual stress contribution generally breaks the initial material symmetries defined by $\mathbf{H}_\parallel$ and $\mathbf{H}_\perp$. Judging from the stress–strain curve alone, the effects of stress softening and permanent set interact and the conjunctive tuning of $\theta_{\mathrm{m},\infty}$ and $\theta_{\mathrm{r},\infty}$ can create a variety of material behaviors during unloading and reloading.

Remark 10. For an incompressible neo-Hookean material, $\Psi_{\text{iso}}^{0,\infty} = \mu(\operatorname{tr}\overline{\mathbf{C}} - 3)/2$ and it follows that $\overline{\mathbf{S}}^{\mathrm{r},\infty} = -\mu\mathbf{I}$ and $\dot{\Psi}_{\text{iso}}^{0,\infty} \equiv -\overline{\mathbf{S}}^{\mathrm{r},\infty} : \dot{\overline{\mathbf{C}}}/2$. The residual stress contribution does not become path-dependent regardless of η_r and, consequently, $w_{\text{cycle}} \equiv 0$, i.e. no permanent set occurs. This is not a problem for the hyperelastic formulation introduced in Section 3.2, since it cannot be reduced to a neo-Hookean model by any combination of material parameters $\theta_{0,\infty}$.

Remark 11. Another way of looking at (48) is that realizations of η_r and $\overline{\mathbf{S}}^{\mathrm{r},\infty} : \dot{\overline{\mathbf{C}}}/2$ are uncorrelated for a random deformation path in an unloading–reloading cycle.

Remark 12. In (48), for the case $\overline{\mathbf{C}} = \overline{\mathbf{C}}^\star$, i.e. the unloading–reloading cycle starts and ends in the same configuration, we get $\mathbb{E}\big[w_{\text{cycle}}\big] = 0$. This coincides with the intuition gained from the example in Section 5.2, where any unloading–reloading cycle can be traversed in either direction, providing either a negative or a positive contribution.

6. Finite linear viscoelasticity

This section deals with the introduction of viscoelasticity to the constitutive model. For the most part, it can be treated independently from the previous two sections on stress softening and permanent set. As before, we start out in a general manner, albeit already with several restrictions compared to the extensive discussion in Liu et al. (2021), which the authors highly recommend. We then specify the resulting expressions for the free-energy function introduced in Section 3 and visualize the stress response in different transient load cases.

By adapting Liu et al. (2021, eqs. 2.37, 2.41, 2.51, 2.55), we define the total isochoric free-energy function as the sum of an equilibrium part $\Psi_{\text{iso}}^{\infty}$ and the non-equilibrium parts Y_l. *Ad hoc*,

$$\begin{aligned}\Psi_{\text{iso}}(\overline{\mathbf{C}}, \overline{\mathbf{C}}^\star, \boldsymbol{\Gamma}_1, \dots, \boldsymbol{\Gamma}_M) &= \Psi_{\text{iso}}^{\infty}(\overline{\mathbf{C}}, \overline{\mathbf{C}}^\star) + \sum_{l=1}^{M} Y_l(\overline{\mathbf{C}}, \boldsymbol{\Gamma}_l) \\ &= \Psi_{\text{iso}}^{\infty}(\overline{\mathbf{C}}, \overline{\mathbf{C}}^\star) + \sum_{l=1}^{M} \frac{1}{4\mu_l'}\left|\beta_l \overline{\mathbf{S}}^{0,\infty}(\overline{\mathbf{C}}) - \mu_l'(\boldsymbol{\Gamma}_l - \mathbf{I})\right|^2,\end{aligned} \tag{55}$$

where $|(\cdot)|^2 = (\cdot) : (\cdot)$ and M denotes the total number of viscous Maxwell elements, each with a stiffness-like parameter μ_l' and a right Cauchy–Green-like internal variable $\boldsymbol{\Gamma}_l$. The dimensionless constant β_l is a strain–energy factor, cf. Govindjee and Simo (1992, eq. 16). Note that μ_l' are different quantities than $\mu_\parallel$ and $\mu_\perp$.

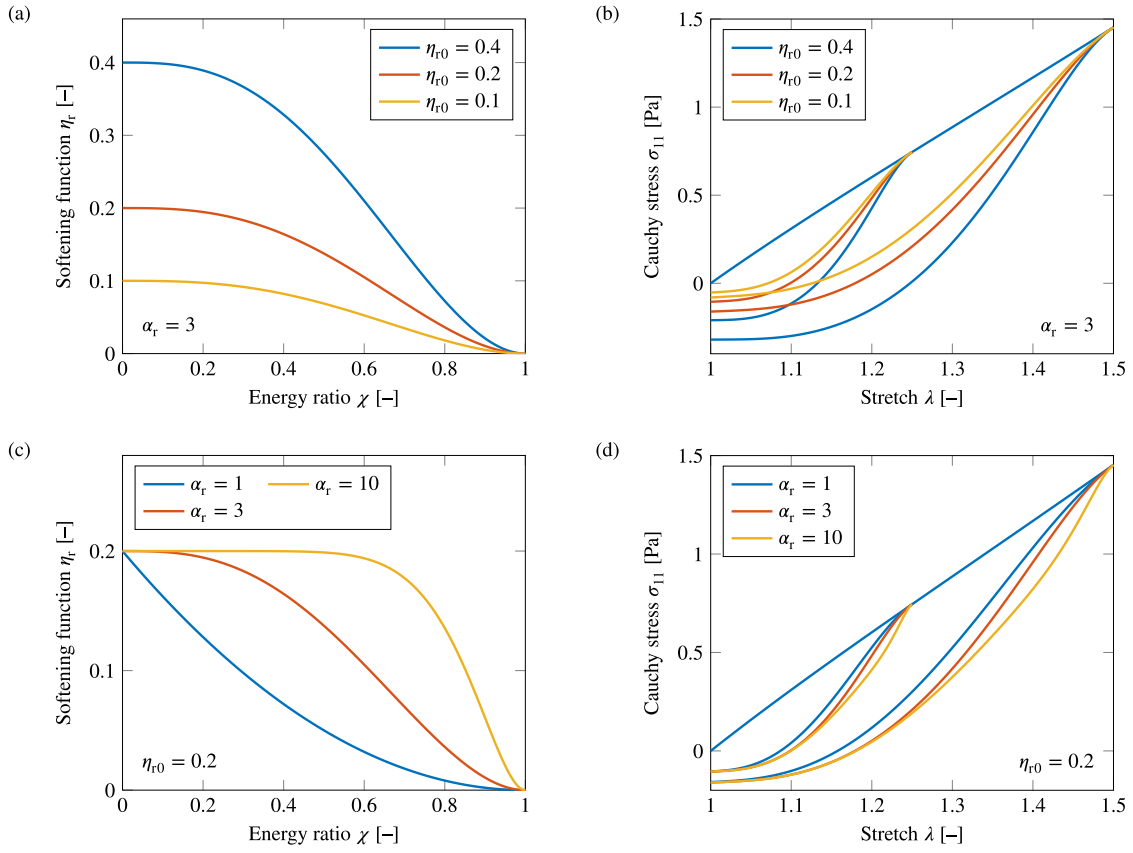

Fig. 4. Three examples for (a) the trajectory of the softening function which models the permanent set for constant α_r and changing η_{r0} and (b) the quasi-static, cyclic, uniaxial stress response given the softening functions from (a). Analogously, three examples for (c) the trajectory of the softening function which models the permanent set for constant η_{r0} and changing α_r and (d) the quasi-static, cyclic, uniaxial stress response given the softening functions from (c). The other material parameters are kept constant with $\theta_{0,\infty} = (0.7, 0.3, 1\,\text{Pa}, 0.2\,\text{Pa}, 0, 0, 0, 0)$ and $\theta_{m,\infty} = (0.1, 1)$.

The thermodynamic discussion for the equilibrium part, presented above, applies analogously here. Therefore, our focus in this section is solely on the non-equilibrium parts. More precisely, we concentrate on a single Maxwell element due to the linearity of the problem. By inserting Y_l into (4), we get the reduced dissipation according to

$$D_{\text{neq}} = -\frac{1}{2\mu_l'}\left[\beta_l \overline{\mathbf{S}}^{0,\infty} - \mu_l'(\boldsymbol{\Gamma}_l - \mathbf{I})\right] : \left(\beta_l \dot{\overline{\mathbf{S}}}^{0,\infty} - \mu_l' \dot{\boldsymbol{\Gamma}}_l\right) \geq 0. \tag{56}$$

By taking a closer look at the term

$$\frac{1}{2}\left[\beta_l \overline{\mathbf{S}}^{0,\infty} - \mu_l'(\boldsymbol{\Gamma}_l - \mathbf{I})\right] : \dot{\boldsymbol{\Gamma}}_l \geq 0, \tag{57}$$

we can ensure positive dissipation by defining the following evolution equation

$$\eta_l \dot{\boldsymbol{\Gamma}}_l = \beta_l \overline{\mathbf{S}}^{0,\infty} - \mu_l'(\boldsymbol{\Gamma}_l - \mathbf{I}) \tag{58}$$

with the viscosity parameter $\eta_l \geq 0$ of the lth Maxwell element. For us, $\overline{\mathbf{S}}^{0,\infty}\big|_{t=0} = \mathbf{0}$ and thus the initial conditions are $\boldsymbol{\Gamma}_l\big|_{t=0} = \mathbf{I}$ and $\dot{\boldsymbol{\Gamma}}_l\big|_{t=0} = \mathbf{0}$. Using the auxiliary non-equilibrium stress tensor $\mathbf{Q}_l = \beta_l \overline{\mathbf{S}}^{0,\infty} - \mu_l'(\boldsymbol{\Gamma}_l - \mathbf{I})$ and the relaxation time $\tau_l = \eta_l/\mu_l'$, we rewrite the evolution equation in the form

$$\dot{\mathbf{Q}}_l + \frac{\mathbf{Q}_l}{\tau_l} = \beta_l \dot{\overline{\mathbf{S}}}^{0,\infty} \tag{59}$$

with $\mathbf{Q}_l\big|_{t=0} = \mathbf{0}$ and $\dot{\mathbf{Q}}_l\big|_{t=0} = \mathbf{0}$, which can be numerically integrated as described in Holzapfel (2000, eq. 6.267) and shown in Appendix D.

The second remaining term in the reduced dissipation (56) is

$$-\frac{\beta_l}{2\mu_l'}\left[\beta_l \overline{\mathbf{S}}^{0,\infty} - \mu_l'(\boldsymbol{\Gamma}_l - \mathbf{I})\right] : \dot{\overline{\mathbf{S}}}^{0,\infty} = -\frac{\beta_l}{2\mu_l'}\mathbf{Q}_l : \dot{\overline{\mathbf{S}}}^{0,\infty} = -\frac{\beta_l}{\mu_l'}\mathbf{Q}_l : \frac{\partial^2 \Psi_{\text{iso}}^{0,\infty}}{\partial \overline{\mathbf{C}} \partial \overline{\mathbf{C}}} : \dot{\overline{\mathbf{C}}}, \tag{60}$$

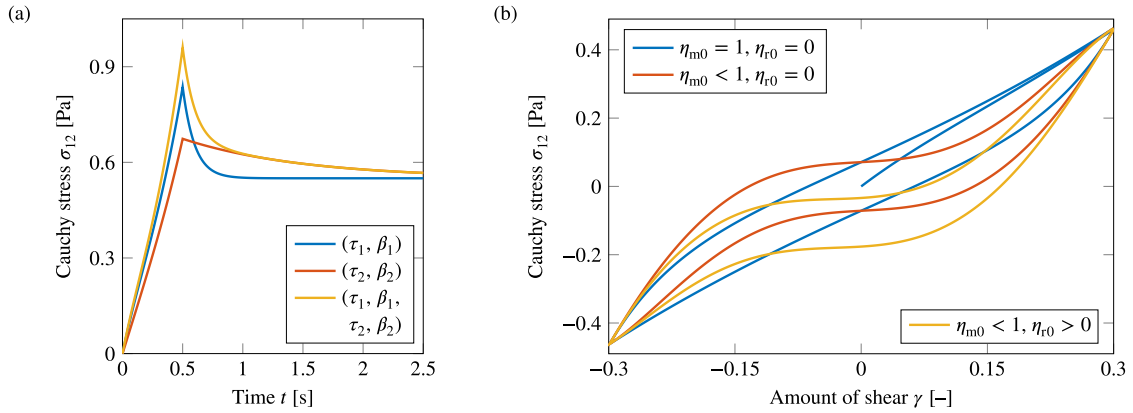

Fig. 5. (a) Relaxation after a simple shear loading for different combinations of Maxwell elements, where $\tau_1 = 0.1\,\mathrm{s}$, $\beta_1 = 0.8$, $\tau_2 = 1\,\mathrm{s}$, and $\beta_2 = 0.3$, and (b) the viscoelastic, cyclic simple shear stress response with and without stress softening and/or permanent set for $\theta_{\mathrm{neq}} = (0.1\,\mathrm{s}, 0.8)$. Otherwise, $\theta_{0,\infty} = (0.7, 0.3, 1\,\mathrm{Pa}, 0.2\,\mathrm{Pa}, 0, 0, 0, 0)$, $\theta_{\mathrm{m},\infty} = (0.1, 1)$, and $\theta_{\mathrm{r},\infty} = (0.3, 1)$.

which can be bracketed with $\dot{\overline{\mathbf{C}}}$. Thus, the term can be associated with the $\overline{\mathbf{S}}$ and in turn with $\mathbf{S}_{\mathrm{iso}}$. Due to the underlying linearity, we define

$$\overline{\mathbf{S}}^{\mathrm{neq}} = 2\frac{\partial^2 \Psi_{\mathrm{iso}}^{0,\infty}}{\partial \overline{\mathbf{C}} \partial \overline{\mathbf{C}}} : \sum_{l=1}^{M} \frac{\beta_l}{\mu_l'} \mathbf{Q}_l, \tag{61}$$

which results in the total second Piola–Kirchhoff stress tensor

$$\mathbf{S} = J^{-2/3}\mathbb{P} : \overline{\mathbf{S}} + \mathbf{S}_{\mathrm{vol}}^{0,\infty} = J^{-2/3}\mathbb{P} : \left(\eta_{\mathrm{m}} \overline{\mathbf{S}}^{0,\infty} + \eta_{\mathrm{r}} \overline{\mathbf{S}}^{\mathrm{r},\infty} + \overline{\mathbf{S}}^{\mathrm{neq}}\right) + \mathbf{S}_{\mathrm{vol}}^{0,\infty} \tag{62}$$

including all constitutive effects. By differentiating (15) with respect to $\overline{\mathbf{C}}$ and subsequent insertion into (61), the fictitious non-equilibrium stress can written explicitly as

$$\overline{\mathbf{S}}^{\mathrm{neq}} = \sum_{p=\{\parallel,\perp\}} \mu_p \Big[\gamma_p \overline{K}_{1p}^{\gamma_p - 1} (\mathbf{H}_p : \mathbf{Q}) \mathbf{H}_p + \delta_p \overline{K}_{-1p}^{\delta_p - 1} \left(\mathbf{H}_p' : \mathbf{Q}\right) \mathbf{H}_p' + \overline{K}_{-1p}^{\delta_p} \left(\overline{\mathbf{C}}^{-1} \mathbf{Q} \mathbf{H}_p' + \mathbf{H}_p' \mathbf{Q} \overline{\mathbf{C}}^{-1} \right) \Big], \tag{63}$$

where

$$\mathbf{Q} = \sum_{l=1}^{M} \frac{\beta_l}{\mu_l'} \mathbf{Q}_l \qquad \text{and} \qquad \mathbf{H}_p' = \overline{\mathbf{C}}^{-1} \mathbf{H}_p \overline{\mathbf{C}}^{-1}. \tag{64}$$

The quantity $\mathbf{Q}/2$ can be interpreted as an elastic Green–Lagrange strain acting on the fourth-order stiffness tensor derived from $\Psi_{\mathrm{iso}}^{0,\infty}$ in (61).

Upon closer inspection of $\mathbf{Q}$ and (59), it can be checked that β_l and μ_l' are not independent parameters for the purposes of computing $\overline{\mathbf{S}}^{\mathrm{neq}}$ due to the linearity of the evolution equation and the subsequent summation; for some choice β_l^*, the parametrizations

$$\left(\beta_l = \beta_l^*, \mu_l' = 1\,\mathrm{Pa}\right) \qquad \text{and} \qquad \left(\beta_l = 1, \mu_l' = \beta_l^{*-2}\,\mathrm{Pa}\right) \tag{65}$$

result in the same values for $\overline{\mathbf{S}}^{\mathrm{neq}}$. The second parameter is however required for an interpretation of thermodynamic quantities such as Y_l. We emphasize that the material constant μ_l' does not directly represent the stiffness of a spring in the lth Maxwell element. Rather, for a fixed value of β_l,

$$\mu_l' \propto \frac{\text{ground stiffness} \times \text{ground stiffness}}{\text{stiffness of the } l\text{th Maxwell element}}, \tag{66}$$

i.e. the larger μ_l', the smaller the viscous stress contribution of the lth element, and *vice versa*.

For the purposes of stress computation, we set $\mu_l' = 1\,\mathrm{Pa}$ without loss of generality. Then each Maxwell element is governed by two independent material parameters, i.e. $\theta_{\mathrm{neq}} = (\tau_1, \beta_1, \ldots, \tau_l, \beta_l, \ldots, \tau_M, \beta_M)$, which brings the total number of material parameters of the constitutive model to $12 + 2M$. Fig. 5(a) shows the relaxation behavior of a specimen after monotonic simple shear up to an amount $\gamma = 0.5$ at a constant rate $\dot{\gamma} = 1\ \mathrm{s}^{-1}$ for different combinations of Maxwell elements. Evidently, the relaxation time τ_l governs the return to the equilibrium configuration as well as the magnitude the viscous overstress alongside β_l. An illustration of the interplay between damage and viscoelasticity is visualized in Fig. 5(b) for cyclic simple shear deformation at $|\dot{\gamma}| = 1\ \mathrm{s}^{-1}$. In both cases the shear mode is '12'.

Remark 13. Although there are considerable similarities between this theory of viscoelasticity and its infinitesimal counterpart, to the authors' knowledge there is generally no corresponding spring–dashpot representation of the former.

Table 1
Expressions and material parameters $\theta_{0,\infty}$ needed for the computation of the polyconvex free-energy function $\Psi_{\text{iso}}^{0,\infty}$ in (9) and the fictitious elastic stress response $\overline{\mathbf{S}}^{0,\infty}$ from (15). If the global coordinate system $(\boldsymbol{E}_k)_{k=1}^3$ coincides with the (initial) planes of material symmetry, the structure tensors $\mathbf{H}_\parallel$ and $\mathbf{H}_\perp$ have a diagonal matrix representation, i.e. $\mathbf{L}_k = \boldsymbol{E}_k \otimes \boldsymbol{E}_k$.

Computationally relevant expressions: (6), (8), (9), (10), and (15)			
Parameter	Bounds	Unit	Interpretation
$\mathbf{L}_k$	n.a.	[–]	Coordinate system, i.e. projection tensors, defining the planes of material symmetry
H_1	$0 \le H_1 \le 1$ $H_1 + H_2 \le 1$	[–]	Measure of fiber orientation associated with the projection tensor $\mathbf{L}_1$
H_2	$0 \le H_2 \le 1$ $H_1 + H_2 \le 1$	[–]	Measure of fiber orientation associated with the projection tensor $\mathbf{L}_2$
$\mu_\parallel$	$\mu_\parallel > 0$	[Pa]	Coaxial stiffness along the fiber direction
$\gamma_\parallel$	$\gamma_\parallel \ge 0$	[–]	Shape parameter associated with the deformation of a line element along the fiber direction
$\delta_\parallel$	$\delta_\parallel \ge 0$	[–]	Shape parameter associated with the deformation an area element along the fiber direction
$\mu_\perp$	$\mu_\perp > 0$	[Pa]	Transverse stiffness perpendicular to the fiber direction
$\gamma_\perp$	$\gamma_\perp \ge 0$	[–]	Shape parameter associated with the deformation of a line element perpendicular to the fiber direction
$\delta_\perp$	$\delta_\perp \ge 0$	[–]	Shape parameter associated with the deformation of an area element perpendicular to the fiber direction

Remark 14. As mentioned in Liu et al. (2021, rem. 10), an incompressible neo-Hookean model with $\dot{\overline{\mathbf{S}}}^{0,\infty} \equiv \mathbf{0}$ never produces a viscoelastic response, which is not an issue for the hyperelastic formulation from Section 3.2, see Remark 10.

Remark 15. This modeling strategy does not require the use of the elastic fictitious stress tensor $\overline{\mathbf{S}}^{0,\infty}$ in (55). Alternatively, one could have chosen $\overline{\mathbf{S}}^{\infty} = \eta_{\text{m}}\overline{\mathbf{S}}^{0,\infty} + \eta_{\text{r}}\overline{\mathbf{S}}^{\text{r},\infty}$ instead, which essentially couples the damage model with the viscoelastic response. Although thermodynamically sound, this choice leads to unphysical material behavior. From (61) we can interpret the non-equilibrium stress $\overline{\mathbf{S}}^{\text{neq}}$ as a product of an elastic Green–Lagrange strain $\mathbf{Q}/2$ with a fourth-order stiffness tensor. If we included the damaged, quasi-static effects in the definition of said stiffness tensor, we would see a stark increase in stiffness with each switch from loading to unloading. The strain-like quantity $\mathbf{Q}/2$ reacts to this change with a delay. The result is a sharp increase in $\overline{\mathbf{S}}^{\text{neq}}$ around the switch from loading to unloading, which cannot be observed experimentally. In general, though, from a thermodynamic perspective, one is unrestricted to choose any such relation independently of the actual quasi-static stress response, as long as the dissipative contribution of potential internal variables thereof remains non-negative.

7. Model summary and calibration outlook

Because the model combines several constitutive effects, we revisit the key expressions needed to calculate a stress response. Furthermore, we summarize all the material parameters involved. Their numbers may seem overwhelming at first, but there are three things to keep in mind. First, the model attempts to describe a material that shows stress softening, permanent set, and viscoelasticity at large strains for select classes of anisotropy, which *per se* necessitates a base amount of parameters. Second, the number of material constants per constitutive effect already tends toward the low end, as emphasized in the remainder of this section. Finally, the interpretability of the various parameters leads to a systematic way of acquiring them through experimental design.

7.1. Model summary

In Section 3.1, we introduce structure tensors to describe anisotropy. In the case of orthotropy, a second-order structure tensor is required with three distinct eigenvalues and a coordinate system defining the planes of material symmetry, i.e. three independent parameters, see (6). With its normalized trace, no fewer than five parameters suffice to define a structure tensor for orthotropy. Two interdependent structure tensors $\mathbf{H}_\parallel$ and $\mathbf{H}_\perp$ help to quantify the coaxial and transverse material behavior, see (8).

Both structure tensors $\mathbf{H}_\parallel$ and $\mathbf{H}_\perp$ are then used to define four isochoric invariants $\overline{K}_{1\parallel}$, $\overline{K}_{-1\parallel}$, $\overline{K}_{1\perp}$, and $\overline{K}_{-1\perp}$, see (10) in Section 3.2. These in turn define the polyconvex free-energy function $\Psi_{\text{iso}}^{0,\infty}$ in (9). To allow sufficient functional generality, each invariant has a shape parameter, i.e. $\gamma_\parallel$, $\delta_\parallel$, $\gamma_\perp$, and $\delta_\perp$, controlling its influence during finite deformations. With the requirement of a stress-free initial configuration, two stiffnesses $\mu_\parallel$ and $\mu_\perp$ remain to govern magnitude of the fictitious elastic stress response $\overline{\mathbf{S}}^{0,\infty}$ from (15). Anything less than these six material constants would involve additional interdependencies between the invariants. Table 1 summarizes $\theta_{0,\infty} = (H_1, H_2, \mu_\parallel, \mu_\perp, \gamma_\parallel, \gamma_\perp, \delta_\parallel, \delta_\perp)$ and the relevant expressions. The underlying assumption of incompressibility must be enforced either with a Lagrange multiplier or a penalty function.

For the modeling of stress softening, the relevant expressions are the definition of the maximally attained 'undamaged' isochoric free energy $\Psi_{\text{iso}}^{\max}$ in (23), the definition of the energy ratio χ and the softening function η_{m} in (30), and the fictitious stiffness-reduced stress response $\eta_{\text{m}}\overline{\mathbf{S}}^{0,\infty}$ from (24). The softening function η_{m} requires two parameters $\theta_{\text{m},\infty} = (\eta_{\text{m}0}, \alpha_{\text{m}})$ controlling the magnitude of damage and the evolution of the stress softening, respectively.

To additionally describe permanent set, we need to keep track of the deformation state $\overline{\mathbf{C}}^*$ associated with $\Psi_{\text{iso}}^{\max}$, as defined in (34). The residual stress contribution $\overline{\mathbf{S}}^{\text{r},\infty}$ then follows from (40), which together with the softening function η_{r} in (54) is added

Table 2
Expressions and material parameters $\theta_{\mathrm{m},\infty}$ and $\theta_{\mathrm{r},\infty}$ needed for the computation of the fictitious stiffness-reduced and residual stress distribution, $\eta_{\mathrm{m}}\overline{\mathbf{S}}^{0,\infty}$ in (24) and $\eta_{\mathrm{r}}\overline{\mathbf{S}}^{\mathrm{r},\infty}$ in (35), respectively.

Computationally relevant expressions: (23), (24), (30), (34), (35), (40), and (54)			
Parameter	Bounds	Unit	Interpretation
$\eta_{\mathrm{m}0}$	$0 < \eta_{\mathrm{m}0} \leq 1$	[–]	Maximum loss of stiffness
α_{m}	$\alpha_{\mathrm{m}} \geq 1$	[–]	Shape parameter associated with the evolution of the stiffness degradation during unloading–reloading
$\eta_{\mathrm{r}0}$	$\eta_{\mathrm{r}0} \geq 0$	[–]	Maximum residual stress contribution
α_{r}	$\alpha_{\mathrm{r}} \geq 1$	[–]	Shape parameter associated with the evolution of the residual stress contribution during unloading–reloading

Table 3
Expressions and material parameters θ_{neq} needed for the computation of the fictitious non-equilibrium stress $\overline{\mathbf{S}}^{\mathrm{neq}}$ in (63). The parameters β_l and μ_l' are interdependent, see (65).

Computationally relevant expressions: (59), (63), and (64)			
Parameter	Bounds	Unit	Interpretation
τ_l	$\tau_l > 0$	[s]	Relaxation time of the lth Maxwell element
β_l	$\beta_l \geq 0$	[–]	Strain-energy factor of the lth Maxwell element scaling the non-equilibrium stress contribution
μ_l'	$\mu_l' \geq 0$	[Pa]	Stiffness-like parameter of the lth Maxwell element scaling the non-equilibrium stress contribution

to the fictitious stress response as $\eta_{\mathrm{r}}\overline{\mathbf{S}}^{\mathrm{r},\infty}$, see (35). Analogous to η_{m}, the softening function η_{r} is parametrized by two constants, namely $\theta_{\mathrm{r},\infty} = (\eta_{\mathrm{r}0}, \alpha_{\mathrm{r}})$, which govern the magnitude and evolution of the residual stress contribution, respectively. All relevant expressions and parameters are listed in Table 2.

For viscoelasticity, every Maxwell element has three material parameters τ_l, β_l, and μ_l', although the last two are interdependent, see (65). The characteristic time τ_l governs the relaxation behavior, while β_l and μ_l act as weights in the calculation of $\mathbf{Q}$ in (64) after solving M evolution Eqs. (59), one for each Maxwell element. The fictitious non-equilibrium stress response $\overline{\mathbf{S}}^{\mathrm{neq}}$ then follows from (63). Without loss of generality, we can choose $\mu_l' = 1\,\mathrm{Pa}$ and consequently $\theta_{\mathrm{neq}} = (\tau_1, \beta_1, \ldots, \tau_l, \beta_l, \ldots, \tau_M, \beta_M)$. As with the previous constitutive effects, the relevant expressions and material parameters are summarized in Table 3.

7.2. Calibration outlook

Although the model can already be used to study the consequences and interactions of the different constitutive effects in a qualitative manner, a calibration needs to be performed to infer any quantitative predictions. A discussion of the intricacies of fitting and the actual acquisition of experimental data is beyond the scope of this work, but we still want to provide a pathway to identify the various material parameters. The modular structure of the constitutive model offers a systematic framework. By precisely designing the loading protocols in mechanical experiments, the contribution of certain constitutive effects can be singled out and treated separately. This of course assumes that the material behaves according to the theory presented here, but this epistemological problem of circular reasoning is unavoidable in experimental design, see the Duhem–Quine thesis, e.g., in Duhem (1976, sec. 2).

The probabilistic interpretation of the structure tensor $\mathbf{H}_{\|}$ in (7) allows for the identification of the anisotropy without the need to perform mechanical experiments, if the orientation distribution $\rho(\boldsymbol{N})$ can be acquired through, e.g., imaging of the microstructure. If such a structural investigation is not possible, the structure tensor $\mathbf{H}_{\|}$ is included in the calibration as an additional set of five parameters that have to be fitted by mechanical experiments. If initial planes of symmetry are assumed *a priori*, the coordinate system is no longer an unknown and only the eigenvalues H_1 and H_2 have to be determined implicitly, see Remark 1.

The fundamental part of the constitutive model is the anisotropic hyperelastic formulation (9) and is parametrized by $\theta_{0,\infty}$, where H_1 and H_2 can also either be prescribed or replaced by $\mathbf{H}_{\|}$, depending on prior assumptions about the anisotropy. We can calibrate $\theta_{0,\infty}$ by using any set of measurements from a quasi-static mechanical experiment in which data associated with primary loading is straightforward to identify, such as uniaxial or equibiaxial extension. A quasi-static loading ensures negligible viscoelastic contributions and confinement to data on the primary loading path prevents overlap with the constitutive models for the damage-related effects. Consequently, $\theta_{0,\infty}$ can be identified independently from $\theta_{\mathrm{m},\infty}$, $\theta_{\mathrm{r},\infty}$, and θ_{neq}. This is a calibration task of comparable complexity to the parameter identification of common isotropic models such as a multi-term Ogden model, cf. Kalina et al. (2020, sec. 3.2.2).

The four parameters of stress softening and permanent set, $\theta_{\mathrm{m},\infty}$ and $\theta_{\mathrm{r},\infty}$, can now be determined by holding $\theta_{0,\infty}$ fixed. For this purpose, the previously acquired, quasi-static measurements can simply be reused, albeit now with calibration to the data associated with unloading–reloading. Therefore, it is advantageous to apply cyclic loading in the quasi-static experiments to ensure that both primary loading and unloading–reloading data is available.

Finally, the viscoelastic constants θ_{neq} can be determined by prescribing the already identified material parameters $\theta_{0,\infty}$, $\theta_{\mathrm{m},\infty}$, and $\theta_{\mathrm{r},\infty}$ during the calibration to experimental data with a transient loading, such as relaxation experiments or cyclic loading at different rates of deformation. In general, the appropriate number of Maxwell elements can be chosen heuristically. Even if only a few samples are available, the experiments can be designed in such a way that various constitutive effects can be differentiated, see Haupt (2002, sec. 6.2).

The parameter identification described above has the advantage that the potentially demanding task of calibration is split into three more manageable sub-problems that can be tackled successively. This also simplifies the planning and execution of the actual experiments and increases the confidence in the validity of the resulting set of parameters.

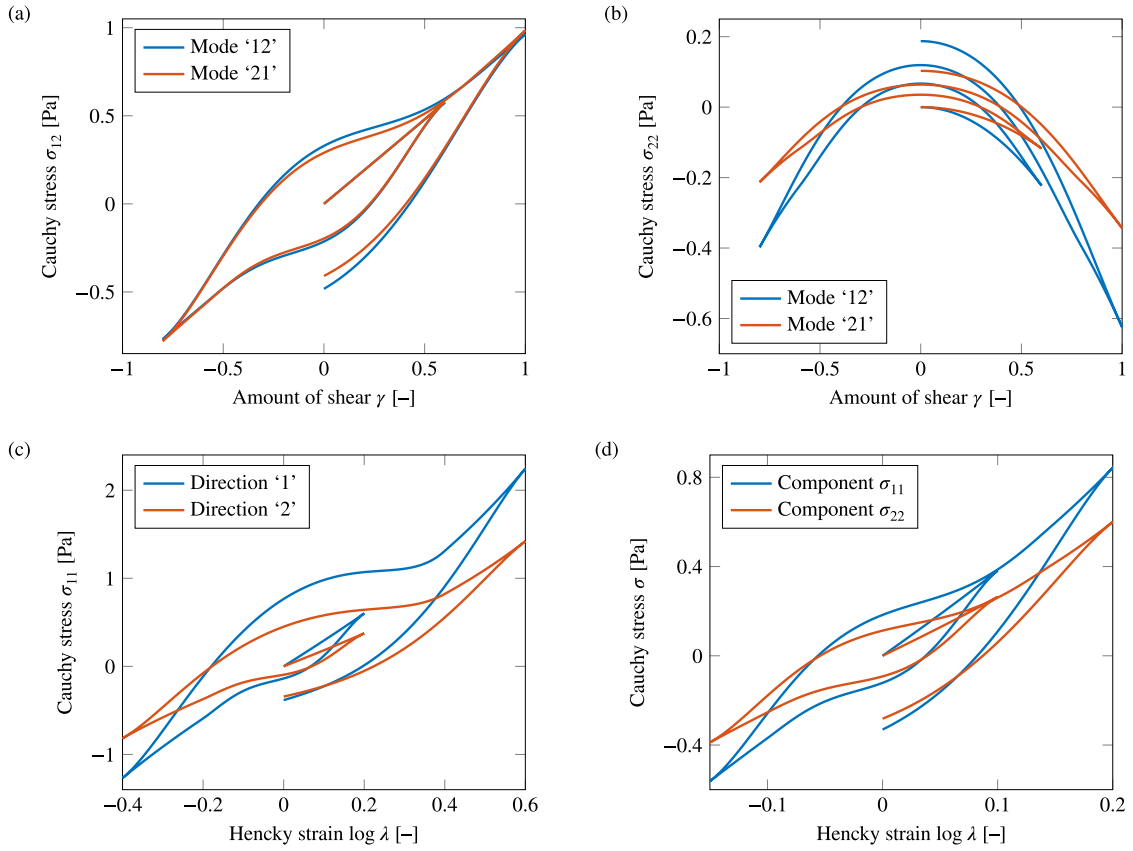

Fig. 6. (a) Shear stress and (b) normal stress response for alternately increasing cyclic simple shear in the '12' and '21' modes, (c) uniaxial response for cyclic tension–compression along the two perpendicular directions '1' and '2', and (d) biaxial response in cyclic tension–compression. Here, the same set of material parameters is used to illustrate the behavior of inelastic effects independent of the deformation mode: $\theta_{0,\infty} = (0.6, 0.3, 1\,\text{Pa}, 0.1\,\text{Pa}, 0, 0, 0, 2)$, $\theta_{\text{m},\infty} = (0.5, 1)$, and $\theta_{\text{r},\infty} = (0.3, 1)$. To avoid visual overload, every boundary-value problem is assumed to be quasi-static, so θ_{neq} is omitted.

8. Further application examples

When a constitutive model is to be used in a real application, it must remain valid for general deformations. Although we attempt to investigate these infinite possibilities through mathematical modeling, we also want to make it explicit for common deformation modes such as simple shear, uniaxial tension–compression, or equibiaxial tension–compression, each with increasing cyclic loading. This applies especially to the pseudo-elastic model for permanent set, which deviates from more classical theories of plasticity involving yield criteria and flow rules. Nonetheless, the approach reproduces physically meaningful constitutive behavior for these deformation modes, which is to be exemplified with a set of parameters that is left constant across the various examples.

Fig. 6(a),(b) show a cube subjected to alternately increasing cyclic, quasi-static simple shear in the '12' and '21' modes, respectively, with damage-related effects enabled. Since the material symmetries align with the reference coordinate system, the shear stress component σ_{12} remains almost identical in both modes during primary loading, until third-order effects become prominent, as proven in Appendix C. In contrast, the normal stress component σ_{22} reveals clear differences for the two shear modes even at smaller values of γ due to anisotropy. The permanent set follows the expected trend, whereby the residual stress contribution progresses for increasing load levels, changing in sign in the case of σ_{12} while remaining monotonic for σ_{22}.

The case of increasing cyclic, quasi-static, uniaxial tension–compression is illustrated in Fig. 6(c), independently of one another along the two perpendicular directions '1' and '2', again, with damage-related effects. A Hencky (true) strain measure is used for appropriate comparability between tension and compression. Here, the anisotropy and the residual stresses are reproduced in a physically meaningful manner, too. Similarly, Fig. 6(d) depicts the stress response in increasing cyclic, quasi-static, equibiaxial tension–compression. In all of these examples it can be seen how the material returns to its initial constitutive behavior upon reentering primary loading.

We would also like to point out a possible shortcoming in the residual stress formulation. Intuitively, the choice to update $\overline{\mathbf{S}}^{\text{r},\infty}$ when a new maximum in $\Psi_{\text{iso}}^{0,\infty}$ is encountered seems reasonable, but can lead to highly sensitive material behavior. An example is a cyclic, quasi-static simple shear deformation with some shear amplitude γ_{amp}. Assuming the material symmetry aligns with the reference coordinate system, $\Psi_{\text{iso}}^{0,\infty}$ is independent of the shearing direction, in contrast to the sign of the shear stress component

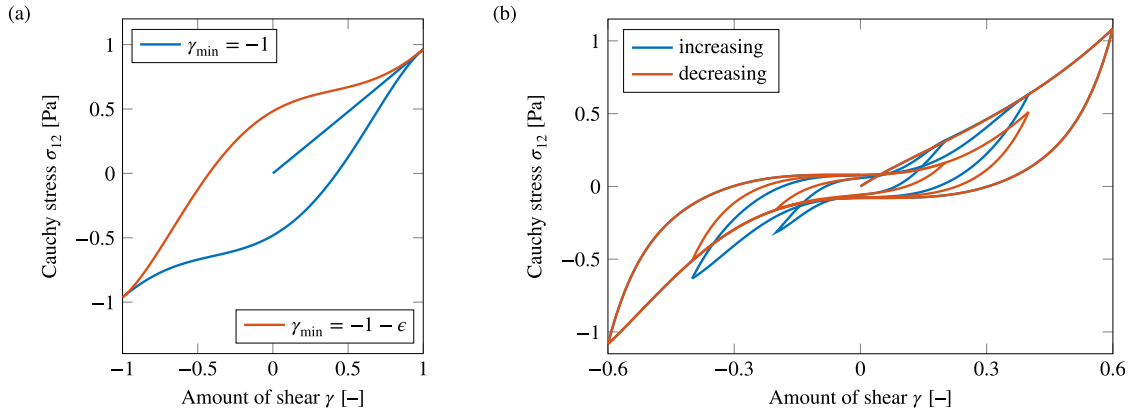

Fig. 7. (a) A cycle in quasi-static simple shear with an amplitude of $\gamma_{\text{amp}} = 1$. If $\gamma_{\min} = -1$, no new maximum is reached in $\Psi_{\text{iso}}^{\max}$ after $\gamma_{\max} = 1$ and the stress trajectory is simply returned along. However, if $\gamma_{\min} = -1 - \epsilon$ with $\epsilon > 0$, the residual shear stress component changes sign, which leads to a completely different behavior in the second half of the cycle. The parameters are the same as in Fig. 6. (b) Stress response for cyclic simple shear, where the amplitudes are prescribed in either increasing or decreasing manner. The material parameters are the same as in Fig. 5(b), but without any residual stress contribution, i.e. $\eta_{\text{r0}} = 0$. The interaction of viscoelasticity and stress softening leads to different responses depending on increasing or decreasing load levels.

$\overline{S}_{12}^{\text{r},\infty}$. Thus, the residual shear stress contribution follows a completely different trajectory, if $\Psi_{\text{iso}}^{\max}$ is only slightly exceeded at the opposite turning point of the cyclic loading, see also Remark 9. This scenario is visualized in Fig. 7(a) for shear mode '12'.

As a final example, Fig. 7(b) depicts the stress response for cyclic simple shear including viscoelasticity at a constant rate $|\dot{\gamma}| = 1\ \text{s}^{-1}$ in mode '12'. Depending on whether the shear levels are prescribed in increasing or decreasing fashion, the result differs in so far as in the former case $\Psi_{\text{iso}}^{\max}$ is updated with each new amplitude, while in the latter case $\Psi_{\text{iso}}^{\max}$ remains constant after the first shear level. This behavior can also be observed experimentally, cf. Nordsletten et al. (2021, fig. 9), which is difficult to reproduce without an interaction of stress softening and viscoelasticity.

9. Conclusion

In this study, we established an anisotropic, incompressible material model capable of reproducing inelastic effects such as viscoelasticity, stress softening, and permanent set at finite strains. Due to its modular structure, each constitutive contribution can be independently tuned by a set of associated, interpretable parameters. Through their interaction, a variety of possible material behaviors can be approximated, at least qualitatively, which has been demonstrated for different modes of deformation. However, we make no claim that the model is able to quantitatively reproduce all experimental data over a large strain range. To this end, more general functional dependencies would have to be allowed, e.g., through approaches like Linka et al. (2021) and Linden et al. (2023). Importantly, such extensions are perfectly in line with the constitutive framework presented here. Any part of the model can be modified, swapped out or, with the exception of the polyconvex free-energy function, disabled.

Each modeling aspect has been independently adapted from existing literature and is built upon in hopes of serving as a possible starting point for further exploration and discussion. While the formulations for the polyconvex free-energy function, stress softening, and finite linear viscoelasticity follow their original publications fairly closely, the introduction of permanent set by a pseudo-elastic framework required more attention. From a heuristic point of view, the constitutive model appears to reproduce physically meaningful residual deformations for a variety of loading protocols and parameter combinations, although we have shown that there must exist deformation paths associated with negative dissipation, or at the very least, negative stress work. In an attempt to explore the apparent validity of the permanent set formulation, we constructed a probabilistic argument to make statements about the stress work of random deformation paths.

The various material parameters of the model are directly associated with the different constitutive effects, which allows for both a direct interpretation and a systematic way of identifying them through experimental design. For an implementation of the material model, only a small number of relationships are necessary to compute a stress response. We briefly summarize the equations required for the algorithmic evaluation of the fictitious stress $\overline{\mathbf{S}}$ in Appendix D. A more detailed discussion of the implementational aspects such as material stiffness, numerical integration of the evolution equation, etc., can be found in a follow-up article by Terzano et al. (2023), which includes the simulation of an application example in a commercial finite element software.

Ultimately, we deem the resulting material model to strike a good balance between descriptive efficacy, mechanical interpretability, and ease of implementation.

CRediT authorship contribution statement

Maximilian P. Wollner: Conceptualization, Formal Analysis, Methodology, Software, Visualization, Writing – original draft. **Michele Terzano:** Supervision, Validation, Writing – original draft. **Malte Rolf-Pissarczyk:** Project Administration, Writing – review & editing. **Gerhard A. Holzapfel:** Supervision, Funding Acquisition, Writing – review & editing.

Declaration of competing interest

The authors declare that they have no known competing financial interests or personal relationships that could have appeared to influence the work reported in this paper.

Data availability

No data was used for the research described in the article.

Acknowledgments

We gratefully acknowledge financial support from the European Union's Horizon 2020 program for research and innovation under grant agreement no. 101017523. In addition, this work was partly funded by Graz University of Technology, Austria, through the LEAD Project on the 'Mechanics, Modeling, and Simulation of Aortic Dissection'. We also thank Dr.-Ing. Stephan Teichtmeister (Graz University of Technology, Austria) for insightful discussions on the foundations of continuum mechanics.

Appendix A. Construction of an unloading–reloading cycle with an unbounded net work

Here we show that given the residual stress formulation (35) it is possible to construct unloading–reloading cycles with an unbounded net work. The starting point is again (38) with $\overline{\mathbf{C}}(t_b) = \overline{\mathbf{C}}(t_a) = \overline{\mathbf{C}}^{\star}$, i.e.

$$w_{\text{cycle}} = \frac{1}{2}\int_{t_a}^{t_b} \eta_{\text{r}}\overline{\mathbf{S}}^{\text{r},\infty} : \dot{\overline{\mathbf{C}}}\,\mathrm{d}\tau. \tag{A.1}$$

Before continuing, we cast (A.1) into a more illustrative form via integration by parts, which yields

$$\begin{aligned}\frac{1}{2}\int_{t_a}^{t_b} \eta_{\text{r}}\overline{\mathbf{S}}^{\text{r},\infty} : \dot{\overline{\mathbf{C}}}\,\mathrm{d}\tau &= \frac{1}{2}\eta_{\text{r}}\overline{\mathbf{S}}^{\text{r},\infty} : \overline{\mathbf{C}}\,\Big|_{t_a}^{t_b} - \frac{1}{2}\int_{t_a}^{t_b} \dot{\eta}_{\text{r}}\overline{\mathbf{S}}^{\text{r},\infty} : \overline{\mathbf{C}}\,\mathrm{d}\tau \\ &= -\frac{1}{2}\int_{t_a}^{t_b} \dot{\eta}_{\text{r}}\overline{\mathbf{S}}^{\text{r},\infty} : \overline{\mathbf{C}}\,\mathrm{d}\tau.\end{aligned} \tag{A.2}$$

Since $\Psi_{\text{iso}}^{0,\infty}(t_a) = \Psi_{\text{iso}}^{0,\infty}(t_b) = \Psi_{\text{iso}}^{\max}$ and $\eta_{\text{r}}(\Psi_{\text{iso}}^{\max}, \Psi_{\text{iso}}^{\max}) = 0$, the first term on the right-hand side disappears.

Then we construct a particular path of deformation $\overline{\mathbf{C}}(\tau)$ for which $w_{\text{cycle}} = 0$. To this end, we split the integral into four parts

$$w_{\text{cycle}} = -\frac{1}{2}\int_{t_a}^{t_b} \dot{\eta}_{\text{r}}\overline{\mathbf{S}}^{\text{r},\infty} : \overline{\mathbf{C}}\,\mathrm{d}\tau = \int_{t_a}^{t_1} \ldots\,\mathrm{d}\tau + \int_{t_1}^{t_2} \ldots\,\mathrm{d}\tau + \int_{t_2}^{t_3} \ldots\,\mathrm{d}\tau + \int_{t_3}^{t_b} \ldots\,\mathrm{d}\tau, \tag{A.3}$$

such that the first interval $\mathcal{T}_{a\to 1}$ and the last interval $\mathcal{T}_{3\to b}$ share the same deformation path, albeit in opposite directions. Hence,

$$\int_{t_a}^{t_1} \ldots\,\mathrm{d}\tau = -\int_{t_3}^{t_b} \ldots\,\mathrm{d}\tau \tag{A.4}$$

and $\overline{\mathbf{C}}(t_1) = \overline{\mathbf{C}}(t_3)$ with $\Psi_{\text{iso}}^{0,\infty}(t_3) = \Psi_{\text{iso}}^{0,\infty}(t_1) < \Psi_{\text{iso}}^{\max}$. Likewise, the two middle contributions $\mathcal{T}_{1\to 2}$ and $\mathcal{T}_{2\to 3}$ are taken to follow an equivalent, but time-reversed deformation path, i.e.

$$\int_{t_1}^{t_2} \ldots\,\mathrm{d}\tau = -\int_{t_2}^{t_3} \ldots\,\mathrm{d}\tau. \tag{A.5}$$

We presuppose that $\Psi_{\text{iso}}^{0,\infty}(t_2) = \Psi_{\text{iso}}^{0,\infty}(t_1)$, but $\overline{\mathbf{C}}(t_2) \neq \overline{\mathbf{C}}(t_1)$. If there is no potential, we can choose $\overline{\mathbf{C}}(\tau)$ in $\mathcal{T}_{1\to 2}$ such that the partial work is non-zero and from (A.5) it follows that

$$\int_{t_1}^{t_2} \ldots\,\mathrm{d}\tau \gtrless 0 \implies \int_{t_2}^{t_3} \ldots\,\mathrm{d}\tau \lesseqgtr 0. \tag{A.6}$$

It is evident that $w_{\text{cycle}} = 0$ by construction.

Now, we slightly alter $\overline{\mathbf{C}}(\tau)$ to define a deformation $\overline{\mathbf{C}}'(\tau)$ in order to produce a non-zero net work w'_{cycle}. Note that in (A.2) we can take any deformation path along an energy contour, where $\Psi_{\text{iso}}^{0,\infty} = \text{const.}$ and therefore $\dot{\eta}_{\text{r}} = 0$, without contributing to the work integral due to the vanishing integrand. Therefore, we can skip the contribution to (A.3) of either $\mathcal{T}_{1\to 2}$ or $\mathcal{T}_{2\to 3}$ as long as $\Psi_{\text{iso}}^{0,\infty}[\overline{\mathbf{C}}'(\tau)] = \text{const.}$ therein, while taking us from $\overline{\mathbf{C}}(t_1)$ to $\overline{\mathbf{C}}(t_2)$ or from $\overline{\mathbf{C}}(t_2)$ to $\overline{\mathbf{C}}(t_3)$, respectively. In the remaining three intervals, $\overline{\mathbf{C}}'(\tau) = \overline{\mathbf{C}}(\tau)$.

It follows that we can always make w'_{cycle} non-zero for a continuous deformation path by skipping or keeping either the contribution from $\mathcal{T}_{1\to 2}$ or $\mathcal{T}_{2\to 3}$, the choice of which defines the sign of w'_{cycle}, see (A.6). Such a strain subcycle, half of it traveling along an energy contour, is itself a closed path of deformation and can be traversed an indefinite number of times, each instance generating a non-zero work contribution. The net work of the entire unloading–reloading cycle is therefore neither bounded from above nor from below.

Let us give an illustrative example for $\overline{\mathbf{C}}(\tau)$ and $\overline{\mathbf{C}}'(\tau)$. Suppose a cube has been extended uniaxially up to a stretch $\lambda_1(t_a)$ reaching some $\Psi_{\text{iso}}^{\max}$ and is therefore residually stressed. Then for $\overline{\mathbf{C}}(\tau)$:

1. $\mathcal{T}_{a\to 1}$: Uniaxial unloading to some stretch $\lambda_1(t_1) < \lambda_1(t_a)$, where $\Psi_{\text{iso}}^{0,\infty}(t_1) < \Psi_{\text{iso}}^{\max}$.
2. $\mathcal{T}_{1\to 2}$: Further uniaxial unloading to some stretch $\lambda_1(t_2) < 1 < \lambda_1(t_1)$ until $\Psi_{\text{iso}}^{0,\infty}(t_2) = \Psi_{\text{iso}}^{0,\infty}(t_1)$ in compression.
3. $\mathcal{T}_{2\to 3}$: Uniaxial reloading until $\lambda_1(t_3) = \lambda_1(t_1)$, where $\Psi_{\text{iso}}^{0,\infty}(t_3) = \Psi_{\text{iso}}^{0,\infty}(t_1)$.
4. $\mathcal{T}_{3\to b}$: Further uniaxial reloading until $\lambda_1(t_b) = \lambda_1(t_a)$.

The resulting net work along $\overline{\mathbf{C}}(\tau)$ is zero. For $\overline{\mathbf{C}}'(\tau)$ we can alter step three in $\overline{\mathbf{C}}(\tau)$:

3. $\mathcal{T}_{2\to 3}$: Biaxial deformation up to $\lambda_1(t_3) = \lambda_1(t_1)$, where $\lambda_2(t)$ is chosen such that $\Psi_{\text{iso}}^{0,\infty}(t) = \text{const}$.

The non-zero contribution in $\mathcal{T}_{2\to 3}$ is skipped, resulting in a non-zero net work along $\overline{\mathbf{C}}'(\tau)$, the sign of which depends on the modeling choice for $\overline{\mathbf{S}}^{\text{r},\infty}$.

Appendix B. Convexity of $\Psi_{\text{iso}}^{0,\infty}$ with respect to $\overline{\mathbf{C}}$

Analogous to Schröder (2010, sec. 5), albeit with respect to $\overline{\mathbf{C}}$, the condition for convexity reads

$$\delta\overline{\mathbf{C}} : \frac{\partial^2 \Psi_{\text{iso}}^{0,\infty}}{\partial\overline{\mathbf{C}}\partial\overline{\mathbf{C}}} : \delta\overline{\mathbf{C}} \geq 0 \quad \forall \overline{\mathbf{C}}, \delta\overline{\mathbf{C}}. \tag{B.1}$$

By routine differentiation of (9), we acquire

$$\frac{\partial \Psi_{\text{iso}}^{0,\infty}}{\partial\overline{\mathbf{C}}} = \frac{1}{2}\sum_{p\in\{\|,\perp\}} \mu_p\left(\overline{K}_{1p}^{\gamma_p}\mathbf{H}_p - \overline{K}_{-1p}^{\delta_p}\overline{\mathbf{C}}^{-1}\mathbf{H}_p\overline{\mathbf{C}}^{-1}\right) \tag{B.2}$$

and after introducing the abbreviation $\mathbf{H}'_p = \overline{\mathbf{C}}^{-1}\mathbf{H}_p\overline{\mathbf{C}}^{-1}$ and differentiating a second time with respect to $\overline{\mathbf{C}}$, we arrive at

$$\frac{\partial^2 \Psi_{\text{iso}}^{0,\infty}}{\partial\overline{\mathbf{C}}\partial\overline{\mathbf{C}}} = \frac{1}{2}\sum_{p\in\{\|,\perp\}} \mu_p\left[\gamma_p\overline{K}_{1p}^{\gamma_p-1}\mathbf{H}_p\otimes\mathbf{H}_p + \delta_p\overline{K}_{-1p}^{\delta_p-1}\mathbf{H}'_p\otimes\mathbf{H}'_p + \overline{K}_{-1p}^{\delta_p}\left(\overline{\mathbf{C}}^{-1}\odot\mathbf{H}'_p + \mathbf{H}'_p\odot\overline{\mathbf{C}}^{-1}\right)\right], \tag{B.3}$$

where $(\cdot)\odot(\cdot)$ denotes the major-symmetric dyadic product, i.e. $[(\cdot)_{IK}(\cdot)_{JL} + (\cdot)_{IL}(\cdot)_{JK}]/2$. Inserting the last expression into condition (B.1) yields

$$\frac{1}{2}\sum_{p\in\{\|,\perp\}} \mu_p\left[\gamma_p\overline{K}_{1p}^{\gamma_p-1}\operatorname{tr}\left(\mathbf{H}_p\delta\overline{\mathbf{C}}\right)^2 + \delta_p\overline{K}_{-1p}^{\delta_p-1}\operatorname{tr}\left(\mathbf{H}'_p\delta\overline{\mathbf{C}}\right)^2 + 2\overline{K}_{-1p}^{\delta_p}\operatorname{tr}\left(\overline{\mathbf{C}}^{-1}\delta\overline{\mathbf{C}}\mathbf{H}'_p\delta\overline{\mathbf{C}}\right)\right] \geq 0 \quad \forall\overline{\mathbf{C}}, \delta\overline{\mathbf{C}}. \tag{B.4}$$

Because the trace of the product of a positive-definite tensor, here $\overline{\mathbf{C}}$ and $\overline{\mathbf{C}}^{-1}$, and a structure tensor $\mathbf{H}_p$ is itself always positive, it follows that the four invariants $\overline{K}_{\pm 1p} > 0$. Likewise, the term $\operatorname{tr}(\overline{\mathbf{C}}^{-1}\delta\overline{\mathbf{C}}\mathbf{H}'_p\delta\overline{\mathbf{C}}) \geq 0$ through the positive semi-definiteness of $\mathbf{H}'_p$. This guarantees the convexity of $\Psi_{\text{iso}}^{0,\infty}$ with respect to $\overline{\mathbf{C}}$, since the expression (B.4) is just a sum of non-negative products given the bounds on the material parameters provided in Section 3.2.

Appendix C. Third-order effects in simple shear

Here we prove the claim that given the hyperelastic formulation in (9), the Cauchy shear stress in modes '12' and '21' during primary loading are identical until third-order effects become relevant. The approach is inspired by the discussion in Truesdell and Noll (1965, sec. 54).

For the constitutive behavior shown in Fig. 6(a), viscoelasticity is omitted and the damage-related effects are switched off during primary loading. The matrix representation of the deformation gradient for simple shear in mode '12' reads

$$[\![\mathbf{F}]\!] = \begin{bmatrix} 1 & \gamma & 0 \\ 0 & 1 & 0 \\ 0 & 0 & 1 \end{bmatrix} \quad \text{and} \quad [\![\mathbf{F}^{-1}]\!] = \begin{bmatrix} 1 & -\gamma & 0 \\ 0 & 1 & 0 \\ 0 & 0 & 1 \end{bmatrix}. \tag{C.1}$$

Since the planes of material symmetry coincide with the global coordinate system, we have

$$[\![\mathbf{H}_\|]\!] = \begin{bmatrix} H_1 & 0 & 0 \\ 0 & H_2 & 0 \\ 0 & 0 & 1-H_1-H_2 \end{bmatrix}. \tag{C.2}$$

Consequently,

$$[\![\mathbf{F}\mathbf{H}_\|\mathbf{F}^{\mathrm{T}}]\!] = \begin{bmatrix} H_1+H_2\gamma^2 & H_2\gamma & 0 \\ H_2\gamma & H_2 & 0 \\ 0 & 0 & 1-H_1-H_2 \end{bmatrix} \quad \Longrightarrow \quad K_{1\|} = 1+H_2\gamma^2, \tag{C.3}$$

$$[\![\mathbf{F}^{-\mathrm{T}}\mathbf{H}_\|\mathbf{F}^{-1}]\!] = \begin{bmatrix} H_1 & -H_1\gamma & 0 \\ -H_1\gamma & H_2+H_1\gamma^2 & 0 \\ 0 & 0 & 1-H_1-H_2 \end{bmatrix} \quad \Longrightarrow \quad K_{-1\|} = 1+H_1\gamma^2, \tag{C.4}$$

and, analogously, for $\mathbf{H}_\perp = (\mathbf{I} - \mathbf{H}_\|)/2$.

Algorithm 1 Computation of fictitious stress $\overline{\mathbf{S}}$

▷ *The history variables are indicated with the subscript 'hist' and are assumed to be properly initialized.* ◁

Require: $\overline{\mathbf{C}}$, Δt, $(\Psi^{\max}_{\mathrm{iso,hist}}, \overline{\mathbf{S}}^{0,\infty}_{\mathrm{hist}}, \overline{\mathbf{S}}^{\mathrm{r},\infty}_{\mathrm{hist}}, \mathbf{Q}_{1,\mathrm{hist}}, \ldots, \mathbf{Q}_{M,\mathrm{hist}})$

▷ *Computation of the undamaged material behavior.* ◁

$\overline{\mathbf{S}}^{0,\infty} \leftarrow \sum_{p\in\{\parallel,\perp\}} \mu_p\left(\overline{K}^{\gamma_p}_{1p}\mathbf{H}_p - \overline{K}^{\delta_p}_{-1p}\overline{\mathbf{C}}^{-1}\mathbf{H}_p\overline{\mathbf{C}}^{-1}\right)$ ▷ *See (15)*

$\Psi^{0,\infty}_{\mathrm{iso}} \leftarrow \frac{1}{2}\sum_{p\in\{\parallel,\perp\}} \mu_p\left[\frac{1}{\gamma_p+1}\left(\overline{K}^{\gamma_p+1}_{1p} - 1\right) + \frac{1}{\delta_p+1}\left(\overline{K}^{\delta_p+1}_{-1p} - 1\right)\right]$ ▷ *See (9)*

▷ *Update of the damage-related history variables.* ◁

if $\Psi^{0,\infty}_{\mathrm{iso}} \geq \Psi^{\max}_{\mathrm{iso,hist}}$ **then**

  $\Psi^{\max}_{\mathrm{iso,hist}} \leftarrow \Psi^{0,\infty}_{\mathrm{iso}}$ ▷ *See (9)*

  $\overline{\mathbf{S}}^{\mathrm{r},\infty}_{\mathrm{hist}} \leftarrow -\overline{\mathbf{S}}^{0,\infty}$ ▷ *See (40)*

$\eta_{\mathrm{m}} \leftarrow \eta_{\mathrm{m0}} + (1-\eta_{\mathrm{m0}})\left[(\alpha_{\mathrm{m}}+1)\chi^{\alpha_{\mathrm{m}}} - \alpha_{\mathrm{m}}\chi^{\alpha_{\mathrm{m}}+1}\right]$ ▷ *See (30)*

$\eta_{\mathrm{r}} \leftarrow \eta_{\mathrm{r0}}\left[1 - (\alpha_{\mathrm{r}}+1)\chi^{\alpha_{\mathrm{r}}} + \alpha_{\mathrm{r}}\chi^{\alpha_{\mathrm{r}}+1}\right]$ ▷ *See (54)*

$\overline{\mathbf{S}}^{\infty} \leftarrow \eta_{\mathrm{m}}\overline{\mathbf{S}}^{0,\infty} + \eta_{\mathrm{r}}\overline{\mathbf{S}}^{\mathrm{r},\infty}_{\mathrm{hist}}$

▷ *Update of viscoelastic history variables.* ◁

for all $l \in \{1, \ldots, M\}$ **do**

  $\mathbf{Q}_{l,\mathrm{hist}} \leftarrow \exp\left(-\frac{\Delta t}{\tau_l}\right)\mathbf{Q}_{l,\mathrm{hist}} + \exp\left(-\frac{1}{2}\frac{\Delta t}{\tau_l}\right)\beta_l\left(\overline{\mathbf{S}}^{0,\infty} - \overline{\mathbf{S}}^{0,\infty}_{\mathrm{hist}}\right)$ ▷ *See (59)*

$\mathbf{Q} \leftarrow \sum_{l=1}^{M} \frac{\beta_l}{\mu'_l}\mathbf{Q}_{l,\mathrm{hist}}$ ▷ *See (64)*

$\overline{\mathbf{S}}^{\mathrm{neq}} \leftarrow \sum_{p=\{\parallel,\perp\}} \mu_p\left[\gamma_p\overline{K}^{\gamma_p-1}_{1p}(\mathbf{H}_p : \mathbf{Q})\mathbf{H}_p + \delta_p\overline{K}^{\delta_p-1}_{-1p}\left(\mathbf{H}'_p : \mathbf{Q}\right)\mathbf{H}'_p + \overline{K}^{\delta_p}_{-1p}\left(\overline{\mathbf{C}}^{-1}\mathbf{Q}\mathbf{H}'_p + \mathbf{H}'_p\mathbf{Q}\overline{\mathbf{C}}^{-1}\right)\right]$ ▷ *See (63)*

$\overline{\mathbf{S}}^{0,\infty}_{\mathrm{hist}} \leftarrow \overline{\mathbf{S}}^{0,\infty}$

▷ *Final computation of the total fictitious stress.* ◁

$\overline{\mathbf{S}} \leftarrow \overline{\mathbf{S}}^{\infty} + \overline{\mathbf{S}}^{\mathrm{neq}}$

return $\overline{\mathbf{S}}$, $(\Psi^{\max}_{\mathrm{iso,hist}}, \overline{\mathbf{S}}^{0,\infty}_{\mathrm{hist}}, \overline{\mathbf{S}}^{\mathrm{r},\infty}_{\mathrm{hist}}, \mathbf{Q}_{1,\mathrm{hist}}, \ldots, \mathbf{Q}_{M,\mathrm{hist}})$

The shear stress component σ_{12} follows as the push-forward of (14) with

$$\sigma_{12}(\gamma) = \mu_{\parallel}\gamma\left[\left(1+H_2\gamma^2\right)^{\gamma_{\parallel}}H_2 + \left(1+H_1\gamma^2\right)^{\delta_{\parallel}}H_1\right] + \mu_{\perp}\gamma\left[\left(1+\frac{1-H_2}{2}\gamma^2\right)^{\gamma_{\perp}}\frac{1-H_2}{2} + \left(1+\frac{1-H_1}{2}\gamma^2\right)^{\delta_{\perp}}\frac{1-H_1}{2}\right]. \tag{C.5}$$

As expected, σ_{12} is an odd function in γ, i.e. $\sigma_{12}(-\gamma) = -\sigma_{12}(\gamma)$. If we expand the expression around $\gamma = 0$, we arrive at

$$\sigma_{12}(\gamma) = \left[\mu_{\parallel}(H_1+H_2) + \mu_{\perp}\left(1 - \frac{H_1+H_2}{2}\right)\right]\gamma + \mathcal{O}(\gamma^3). \tag{C.6}$$

A permutation of H_1 and H_2 is equivalent to a change in simple shear from mode '12' to '21', which is straightforward to verify by carrying out the tensor products (C.3) and (C.4) for simple shear in mode '21' reading

$$[\![\mathbf{F}]\!] = \begin{bmatrix} 1 & 0 & 0 \\ \gamma & 1 & 0 \\ 0 & 0 & 1 \end{bmatrix} \quad \text{and} \quad [\![\mathbf{F}^{-1}]\!] = \begin{bmatrix} 1 & 0 & 0 \\ -\gamma & 1 & 0 \\ 0 & 0 & 1 \end{bmatrix}. \tag{C.7}$$

The linear term in (C.6) is invariant under this operation. Therefore, any differences in the shear stress between modes '12' and '21' are the result of additional terms, i.e. third-order effects, as claimed above.

Appendix D. Algorithm for the computation of the fictitious stress $\overline{\mathbf{S}}$

Here we describe an algorithm for calculating the fictitious stress $\overline{\mathbf{S}}$, which plays the central role in the constitutive model, see (62). The initial values for the history variables are $\Psi^{\max}_{\mathrm{iso,hist}} = 0$ and $\overline{\mathbf{S}}^{0,\infty}_{\mathrm{hist}} = \overline{\mathbf{S}}^{\mathrm{r},\infty}_{\mathrm{hist}} = \mathbf{Q}_{l,\mathrm{hist}} = \mathbf{0}$, although it may be numerically advantageous to choose some $\Psi^{\max}_{\mathrm{iso,hist}} = \epsilon > 0$ to avoid limiting issues in the first increment. The discrete time step of the current increment is denoted by Δt.

References

Baker, B.M., Nerurkar, N.L., Burdick, J.A., Elliott, D.M., Mauck, R.L., 2009. Fabrication and modeling of dynamic multipolymer nanofibrous scaffolds. J. Biomech. Eng. 131 (10), 101012. http://dx.doi.org/10.1115/1.3192140.

Balzani, D., Neff, P., Schröder, J., Holzapfel, G.A., 2006. A polyconvex framework for soft biological tissues. Adjustment to experimental data. Int. J. Solids Struct. 43 (20), 6052–6070. http://dx.doi.org/10.1016/j.ijsolstr.2005.07.048.

Bezanson, J., Edelman, A., Karpinski, S., Shah, V.B., 2017. Julia: A fresh approach to numerical computing. SIAM Rev. Soc. Ind. Appl. Math. 59 (1), 65–98. http://dx.doi.org/10.1137/141000671.

Britt, B.R., Ehret, A.E., 2022. Constitutive modelling of fibre networks with stretch distributions. Part I: Theory and illustration. J. Mech. Phys. Solids 167, 104960. http://dx.doi.org/10.1016/j.jmps.2022.104960.

Casey, J., 2017. A convenient form of the multiplicative decomposition of the deformation gradient. Math. Mech. Solids 22 (3), 528–537. http://dx.doi.org/10.1177/1081286515598662.
Ciambella, J., Nardinocchi, P., 2021. A structurally frame-indifferent model for anisotropic visco-hyperelastic materials. J. Mech. Phys. Solids 147, 104247. http://dx.doi.org/10.1016/j.jmps.2020.104247.
Diani, J., Fayolle, B., Gilmorini, P., 2009. A review on the Mullins effect. Eur. Polym. J. 45 (3), 601–612. http://dx.doi.org/10.1016/j.eurpolymj.2008.11.017.
Dorfmann, A., Ogden, R.W., 2004. A constitutive model for the Mullins effect with permanent set in particle-reinforced rubber. Int. J. Solids Struct. 41 (7), 1855–1878. http://dx.doi.org/10.1016/j.ijsolstr.2003.11.014.
Driessen, N.J.B., Peters, G.W.M., Huyghe, J.M., Bouten, C.V.C., Baaijens, F.P.T., 2003. Remodelling of continuously distributed collagen fibres in soft connective tissues. J. Biomech. 36 (8), 1151–1158. http://dx.doi.org/10.1016/S0021-9290(03)00082-4.
Duhem, P., 1976. Physical theory and experiment. In: Harding, S.G. (Ed.), Can Theories Be Refuted? Essays on the Duhem-Quine Thesis. D. Reidel Publishing Company, pp. 1–40. http://dx.doi.org/10.1007/978-94-010-1863-0_1, chapter 2.
Ehret, A.E., Itskov, M., 2007. A polyconvex hyperelastic model for fiber-reinforced materials in application to soft tissues. J. Mater. Sci. 42, 8853–8863. http://dx.doi.org/10.1007/s10853-007-1812-6.
Eringen, A.C., 1980. Mechanics of Continua, second ed. Robert E. Krieger Publishing Company, Inc..
Evans, M., Hastings, N., Peacock, B., 2000. Statistical Distributions, third ed. John Wiley & Sons, Inc..
Fereidoonnezhad, B., Naghdabadi, R., Holzapfel, G.A., 2016. Stress softening and permanent deformation in human aortas: Continuum and computational modeling with application to arterial clamping. J. Mech. Behav. Biomed. Mater. 61, 600–616. http://dx.doi.org/10.1016/j.jmbbm.2016.03.026.
Fisk, D.L., 1963. Quasi-Martingales and Stochastic Integrals (Ph.D. thesis). Michigan State University, http://dx.doi.org/10.25335/M5D21RX21.
Flory, P.J., 1961. Thermodynamic relations for high elastic materials. Trans. Faraday Soc. 57, 829–838. http://dx.doi.org/10.1039/TF9615700829.
Gasser, T.C., Ogden, R.W., Holzapfel, G.A., 2006. Hyperelastic modelling of arterial layers with distributed collagen fibre orientations. J. R. Soc. Interface 3 (6), 15–35. http://dx.doi.org/10.1098/rsif.2005.0073.
Göktepe, S., Miehe, C., 2005. A micro–macro approach to rubber-like materials. Part III: The micro-sphere model of anisotropic Mullins-type damage. J. Mech. Phys. Solids 53 (10), 2259–2283. http://dx.doi.org/10.1016/j.jmps.2005.04.010.
Govindjee, S., Simo, J.C., 1992. Mullins' effect and the strain amplitude dependence of the storage modulus. Int. J. Solids Struct. 29 (14), 1737–1751. http://dx.doi.org/10.1016/0020-7683(92)90167-R.
Gültekin, O., Dal, H., Holzapfel, G.A., 2019. On the quasi-incompressible finite element analysis of anisotropic hyperelastic materials. Comput. Mech. 63, 443–453. http://dx.doi.org/10.1007/s00466-018-1602-9.
Hartmann, S., Neff, P., 2003. Polyconvexity of generalized polynomial-type hyperelastic strain energy functions for near-incompressibility. Int. J. Solids Struct. 40 (11), 2767–2791. http://dx.doi.org/10.1016/S0020-7683(03)00086-6.
Haupt, P., 2002. Continuum Mechanics and Theory of Materials, second ed. Springer-Verlag Berlin Heidelberg, http://dx.doi.org/10.1007/978-3-662-04775-0.
Hill, R., 1968. On constitutive inequalities for simple materials – I. J. Mech. Phys. Solids 16 (4), 229–242. http://dx.doi.org/10.1016/0022-5096(68)90031-8.
Holthusen, H., Rothkranz, C., Lamm, L., Brepols, T., Reese, S., 2023. Inelastic material formulations based on a co-rotated intermediate configuration—Application to bioengineered tissues. J. Mech. Phys. Solids 172, 105174. http://dx.doi.org/10.1016/j.jmps.2022.105174.
Holzapfel, G.A., 2000. Nonlinear Solid Mechanics: A Continuum Approach for Engineering. John Wiley & Sons, Ltd..
Holzapfel, G.A., Ogden, R.W., 2009. Constitutive modelling of passive myocardium: a structurally based framework for material characterization. Proc. Math. Phys. Eng. Sci. 367 (19023), 3445–3475. http://dx.doi.org/10.1098/rsta.2009.0091.
Holzapfel, G.A., Ogden, R.W., Sherifova, S., 2019. On fibre dispersion modelling of soft biological tissues: a review. Proc. Math. Phys. Eng. Sci. 475 (2224), 20180736. http://dx.doi.org/10.1098/rspa.2018.0736.
Holzapfel, G.A., Simo, J.C., 1996. A new viscoelastic constitutive model for continuous media at finite thermomechanical changes. Int. J. Solids Struct. 33 (20), 3019–3034. http://dx.doi.org/10.1016/0020-7683(95)00263-4.
Humphrey, J.D., 2003. Review paper: Continuum biomechanics of soft biological tissues. Proc. Math. Phys. Eng. Sci. 459 (2029), 3–46. http://dx.doi.org/10.1098/rspa.2002.1060.
Itskov, M., Aksel, N., 2004. A class of orthotropic and transversely isotropic hyperelastic constitutive models based on a polyconvex strain energy function. Int. J. Solids Struct. 41 (14), 3833–3848. http://dx.doi.org/10.1016/j.ijsolstr.2004.02.027.
Itskov, M., Ehret, A., Kazakevičiūtė-Makovska, R., Weinhold, G., 2010. A thermodynamically consistent phenomenological model of the anisotropic Mullins effect. Z. Angew. Math. Mech. 90 (5), 370–386. http://dx.doi.org/10.1002/zamm.200900279.
Kalina, K.A., Raßloff, A., Wollner, M., Metsch, P., Brummund, J., Kästner, M., 2020. Multiscale modeling and simulation of magneto-active elastomers based on experimental data. Phys. Sci. Rev. 8 (1), 1–31. http://dx.doi.org/10.1515/psr-2020-0012.
Krawietz, A., 1986. Materialtheorie. Springer-Verlag Berlin Heidelberg, http://dx.doi.org/10.1007/978-3-642-82512-5.
Lanir, Y., 2017. Multi-scale structural modeling of soft tissues mechanics and mechanobiology. J. Elast. 129, 7–48. http://dx.doi.org/10.1007/s10659-016-9607-0.
Li, W., 2016. Damage models for soft tissues. J. Med. Biol. Eng. 36, 285–307. http://dx.doi.org/10.1007/s40846-016-0132-1.
Li, R.L., Russ, J., Paschalides, C., Ferrari, G., Waisman, H., Kysar, J.W., Kalfa, D., 2019. Mechanical considerations for polymeric heart valve development: Biomechanics, materials, design and manufacturing. Biomaterials 225, 119493. http://dx.doi.org/10.1016/j.biomaterials.2019.119493.
Linden, L., Klein, D.K., Kalina, K.A., Brummund, J., Weeger, O., Kästner, M., 2023. Neural networks meet hyperelasticity: A guide to enforcing physics. J. Mech. Phys. Solids 105363. http://dx.doi.org/10.1016/j.jmps.2023.105363.
Linka, K., Hillgärtner, M., Abdolazizi, K.P., Aydin, R.C., Itskov, M., Cyron, C.J., 2021. Constitutive artificial neural networks: A fast and general approach to predictive data-driven constitutive modeling by deep learning. J. Comput. Phys. 429 (8), 110010. http://dx.doi.org/10.1016/j.jcp.2020.110010.
Liu, J., Latorre, M., Marsden, A.L., 2021. A continuum and computational framework for viscoelastodynamics: I. Finite deformation linear models. Comput. Methods Appl. Mech. Engrg. 385, 114059. http://dx.doi.org/10.1016/j.cma.2021.114059.
Miehe, C., Göktepe, S., Lulei, F., 2004. A micro-macro approach to rubber-like materials—Part I: The non-affine micro-sphere model of rubber elasticity. J. Mech. Phys. Solids 52 (11), 2617–2660. http://dx.doi.org/10.1016/j.jmps.2004.03.011.
Miehe, C., Keck, J., 2000. Superimposed finite elastic–viscoelastic–plastoelastic stress response with damage in filled rubbery polymers. Experiments, modelling and algorithmic implementation. J. Mech. Phys. Solids 48 (2), 323–365. http://dx.doi.org/10.1016/S0022-5096(99)00017-4.
Mullins, L., 1948. Effect of stretching on the properties of rubber. Rubber Chem. Technol. 21 (2), 281–300. http://dx.doi.org/10.5254/1.3546914.
Naumann, C., Ihlemann, J., 2015. On the thermodynamics of pseudo-elastic material models which reproduce the Mullins effect. Int. J. Solids Struct. 69–70, 360–369. http://dx.doi.org/10.1016/j.ijsolstr.2015.05.014.
Nordsletten, D., Capilnasiu, A., Zhang, W., Wittgenstein, A., Hadjicharalambous, M., Sommer, G., Sinkus, R., Holzapfel, G.A., 2021. A viscoelastic model for human myocardium. Acta Biomater. 135, 441–457. http://dx.doi.org/10.1016/j.actbio.2021.08.036.
Ogden, R.W., 1997. Non-Linear Elastic Deformations. Dover Publications, Inc..
Ogden, R.W., Roxburgh, D.G., 1999. A pseudo-elastic model for the Mullins effect in filled rubber. Proc. Math. Phys. Eng. Sci. 455 (1988), 2861–2877. http://dx.doi.org/10.1098/rspa.1999.0431.
Pierrat, B., Nováček, V., Avril, S., Turquier, F., 2021. Mechanical characterization and modeling of knitted textile implants with permanent set. J. Mech. Behav. Biomed. Mater. 114, 104210. http://dx.doi.org/10.1016/j.jmbbm.2020.104210.
Reese, S., 2003. Meso-macro modelling of fibre-reinforced rubber-like composites exhibiting large elastoplastic deformation. Int. J. Solids Struct. 40 (4), 951–980. http://dx.doi.org/10.1016/S0020-7683(02)00602-9.

Reese, S., Govindjee, S., 1998. A theory of finite viscoelasticity and numerical aspects. Int. J. Solids Struct. 35 (26), 3455–3482. http://dx.doi.org/10.1016/S0020-7683(97)00217-5.

Sansour, C., 2008. On the physical assumptions underlying the volumetric-isochoric split and the case of anisotropy. Eur. J. Mech. A Solids 27 (1), 28–39. http://dx.doi.org/10.1016/j.euromechsol.2007.04.001.

Schröder, J., 2010. Anisotropic polyconvex functions. In: Schröder, J., Neff, P. (Eds.), Poly-, Quasi- and Rank-One Convexity in Applied Mechanics. Springer Vienna, pp. 53–105. http://dx.doi.org/10.1007/978-3-7091-0174-2, chapter 3.

Schröder, J., Neff, P., 2003. Invariant formulation of hyperelastic transverse isotropy based on polyconvex free energy functions. Int. J. Solids Struct. 40 (2), 401–445. http://dx.doi.org/10.1016/S0020-7683(02)00458-4.

Simo, J.C., 1987. On a fully three-dimensional finite-strain viscoelastic damage model: Formulation and computational aspects. Comput. Methods Appl. Mech. Engrg. 60 (2), 153–173. http://dx.doi.org/10.1016/0045-7825(87)90107-1.

Szafron, J.M., Ramachandra, A.B., Breuer, C.K., Marsden, A.L., Humphrey, J.D., 2019. Optimization of tissue-engineered vascular graft design using computational modeling. Tissue Eng. C Methods 25 (10), 561–570. http://dx.doi.org/10.1089/ten.tec.2019.0086.

Terzano, M., Wollner, M.P., Rolf-Pissarczyk, M., Kainz, M.P., Götzen, N., Holzapfel, G.A., 2023. Modelling the anisotropic inelastic response of polymeric scaffolds for in situ tissue engineering applications. J. R. Soc. Interface (in press).

Tkachuk, M., Linder, C., 2012. The maximal advance path constraint for the homogenization of materials with random network microstructure. Philos. Mag. (Abingdon) 92 (22), 2779–2808. http://dx.doi.org/10.1080/14786435.2012.675090.

Truesdell, C., Noll, W., 1965. The Non-Linear Field Theories of Mechanics. Springer-Verlag Berlin Heidelberg New York, http://dx.doi.org/10.1007/978-3-662-10388-3.

Vernerey, F.J., 2018. Transient response of nonlinear polymer networks: A kinetic theory. J. Mech. Phys. Solids 115, 230–247. http://dx.doi.org/10.1016/j.jmps.2018.02.018.

Zheng, Q.-S., 1994. Theory of representations for tensor functions – A unified invariant approach to constitutive equations. Appl. Mech. Rev. 47 (11), 545–587. http://dx.doi.org/10.1115/1.3111066.